

Quest for understanding hadrons at low energies: Monte Carlo tools vs. experimental data

S. Actis¹, A. Arbuzov², G. Balossini³, C. Bignamini³, R. Bonciani⁴, C.M. Carloni Calame⁵, M. Czakon⁶, H. Czyz⁷, A. Denig⁸, A. Ferroglia⁹, J. Gluza⁷, A. Hafner⁸, P. Mastrolia¹⁰, G. Montagna³, F. Nguyen¹¹, O. Nicrosini¹², A. Penin¹³, F. Piccinini¹², E. Remiddi¹⁴, T. Riemann¹⁵, A. Sibidanov¹⁶, L. Trentadue¹⁷, J. J. van der Bij¹⁸, P. Wang¹⁹, and M. Worek³

¹ Institut für Theoretische Physik E, RWTH Aachen Universität, D-52056 Aachen, Germany

² Bogoliubov Laboratory of Theoretical Physics, Joint Institute for Nuclear Research, Dubna, Russia

³ Dipartimento di Fisica Nucleare e Teorica, Università di Pavia, and INFN, Sezione di Pavia, I-27100 Pavia, Italy

⁴ Laboratoire de Physique Subatomique et de Cosmologie, Université Joseph Fourier/CNRS-IN2P3/INPG, F-38026 Grenoble, France

⁵ School of Physics and Astronomy, University of Southampton, Highfield, Southampton SO17 1BJ, UK

⁶ Fachbereich C, Bergische Universität Wuppertal, D-42097 Wuppertal, Germany

⁷ Department of Field Theory and Particle Physics, Institut of Physics, University of Silesia, PL-40007 Katowice, Poland

⁸ Institut für Kernphysik, Johannes Gutenberg-Universität Mainz, D-55128 Mainz, Germany

⁹ Institut für Physik (THEP), Johannes Gutenberg-Universität, D-55099 Mainz, Germany

¹⁰ CERN, Theory Department, CH-1211 Genève, Switzerland

¹¹ Dipartimento di Fisica dell'Università Roma Tre, and INFN, Sezione di Roma Tre, I-00146, Roma, Italy

¹² INFN, Sezione di Pavia, I-27100 Pavia, Italy

¹³ Department of Physics, University of Alberta, Edmonton, AB T6G 2J1, Canada

¹⁴ Dipartimento di Fisica dell'Università di Bologna, and INFN, Sezione di Bologna, I-40126 Bologna, Italy

¹⁵ Deutsches Elektronen-Synchrotron, DESY, D-15738 Zeuthen, Germany

¹⁶ Budker Institute of Nuclear Physics, Novosibirsk, 630090 Russia

¹⁷ Dipartimento di Fisica, Università di Parma, and INFN, Gruppo Collegato di Parma I-43100 Parma, Italy

¹⁸ Physikalisches Institut, Albert-Ludwigs-Universität Freiburg, D-79104 Freiburg, Germany

¹⁹ Institute of High Energy Physics, Beijing 10049, People's Republic of China

Received: date / Revised version: date

Abstract. Review of the work done and presented during the workshop “Radiative corrections and generators for low energy hadronic cross section and luminosity” on precision luminosity at meson factories.

PACS. PACS-key describing text of that key – PACS-key describing text of that key

1 Luminosity

The present Section addresses the most important experimental and theoretical issues involved in the precision determination of the luminosity at meson factories. The luminosity is the key ingredient underlying all the measurements and studies of the physics processes discussed in the other Sections. Particular emphasis is put on the theoretical accuracy inherent the event generators used in the experimental analysis, in comparison with the most advanced perturbative calculations and experimental precision requirements. The effort done during the workshop to perform tuned comparisons between the predictions of the most accurate programs is described in detail. New calculations, leading to an update of the theoretical error associated to the prediction of the luminosity cross section, are also presented. The aim of the Section is to

provide a self-contained and up-to-date description of the progress occurred during the last few years towards high-precision luminosity monitoring at flavour factories, as well as of the open issues necessary for future advances.

The structure of the Section is as follows. After an introduction on the motivation for precision luminosity measurements at meson factories (Section 1.1), the leading-order (LO) cross sections of the two QED processes of major interest, i.e. Bhabha scattering and photon pair production, are presented in Section 1.2, together with the formulae for the next-to-leading-order (NLO) corrections to the above processes. The remarkable progress on the calculation of next-to-next-leading-order (NNLO) QED corrections to the Bhabha cross section, as occurred in the last few years, is reviewed in Section 1.4. In particular, this Section presents new, exact results about lepton and hadron pair corrections, taking into account realistic event

selection criteria. Section 1.5 is devoted to the description of the theoretical methods used in the Monte Carlo (MC) generators for the simulation of multiple photon radiation. The matching of such contributions with NLO corrections is also described in Section 1.5. The main features of the MC programs used by the experimental collaborations are summarized in Section 1.6. Numerical results for the radiative corrections implemented into the MC generators are shown in Section 1.7 for both the Bhabha process and two photon production. The tuned comparisons between the predictions of the most precise generators are presented and discussed in detail in Section 1.8, considering the Bhabha process at different center of mass (c.m.) energies and in the presence of realistic experimental cuts. The theoretical accuracy presently reached by the luminosity tools is addressed in Section 1.9, where the most important sources of uncertainty are discussed quantitatively. The estimate of the total error affecting the calculation of the Bhabha cross section is given, as main conclusion of the present work, in Section 1.10, updating and making more robust results available in the literature. Some open issues are drawn in Section 1.10 as well.

1.1 Motivation

The luminosity of a collider is the proportionality constant between the event rate and the cross section of a given process. For an accurate measurement of the cross section of an e^+e^- annihilation process, the precise knowledge of the collider luminosity is mandatory.

The luminosity depends on three factors: beam-beam crossing frequency, beam currents and the beam overlap area in the crossing region. However, the last quantity is difficult to determine accurately from the collider optics. Thus, experiments prefer to determine the luminosity by the counting rate of well selected events whose cross section is known with good accuracy, using the formula

$$\int \mathcal{L} dt = \frac{N}{\sigma} \quad (1)$$

where N and σ are the number of events and the theoretical cross section of the chosen reference process, respectively. Therefore, the total luminosity error will be given by the sum in quadrature of the fractional experimental and theoretical uncertainty.

Since the advent of low luminosity e^+e^- colliders, a great effort was devoted to obtaining good precision in the cross section of electromagnetic processes, extending the pioneering work of the earlier days [1]. At the e^+e^- colliders, operating in the c.m. range $1 \text{ GeV} < \sqrt{s} < 3 \text{ GeV}$, such as ACO at Orsay, VEPP-II at Novosibirsk and Adone at Frascati, the luminosity measurement was based on Bhabha scattering [2, 3] with final state e^\pm detected at small angles, or single and double bremsstrahlung processes [4], thanks to the high statistics. The electromagnetic cross sections scale as $1/s$, while elastic e^+e^- scattering has a steep dependence on the polar angle, $\sim 1/\theta^3$, thus providing high rate for small values of θ .

Also at high energy accelerators LEP at CERN and SLC at Stanford, running in the '90s around the Z pole to perform precision tests of the Standard Model (SM), experiments used small-angle Bhabha scattering events. Indeed, for the very forward angular acceptances considered by LEP/SLC collaborations, the Bhabha process is dominated by the electromagnetic interaction and, therefore, calculable at least in principle, with very high theoretical accuracy. At the end of LEP and SLC operation, a total (experimental plus theoretical) precision of one per mille (or better) was achieved [5, 6, 7, 8], thanks to the work of different theoretical groups and the excellent performance of precision luminometers.

At low and intermediate energy high-luminosity meson factories, the small polar angle region is difficult to access for the presence of the low-beta insertions close to the beam crossing region, while wide-angle Bhabha scattering produce a large counting rate and can be exploited for a precise measurement of the luminosity.

Therefore, also in this latter case of e^\pm scattered at large angles, i.e. 55° for the KLOE experiment [9] running at DAΦNE, Frascati and 40° for the CLEO-c experiment [10] running at CESR, Cornell, the main advantages of Bhabha scattering are preserved:

1. large statistics. For example at DAΦNE, a statistical error $\delta\mathcal{L}/\mathcal{L} \sim 0.3\%$ is reached in about two hours of data taking, even at the lowest luminosities;
2. high theoretical accuracy by which the cross section can be calculated;
3. clean event topology of the signal and small amount of background.

In Eq. (1) the cross section is usually evaluated by inserting event generators, which include radiative corrections at a high level of precision, into the MC code simulating the detector response. This must be developed to reproduce the detector performance (geometrical acceptance, reconstruction efficiency and resolution of the measured quantities) to a high level of confidence.

For most cases of interest, the major source of systematic uncertainty in the experimental measurement of the luminosity is exactly the different efficiency or the different resolution between data and MC.

For the KLOE luminosity measurement, indeed, the largest experimental error is due to a difference in resolution on the polar angle, measured with the calorimeter, that results in a different border effect, between data and MC. Left panel of Fig. 1 shows the very good agreement between data and MC distributions of the e^\pm polar angle, where a fractional difference of $\sim 0.3\%$ still affects the border region, due to the steep behaviour of the distribution. The right panel of Fig. 1 shows the the very good agreement between data and MC in the acollinearity, $\zeta = |\theta_{e^+} + \theta_{e^-} - 180^\circ|$, distribution. In this case, the analysis cut, $\zeta < 9^\circ$ is very far from the bulk of the distribution, and it does introduce negligible systematic effects. Also in the CLEO-c luminosity measurement with Bhabha scattering events, the detector modeling is the main source of experimental error. In particular, uncertainties include those due to finding and reconstruction of the electron

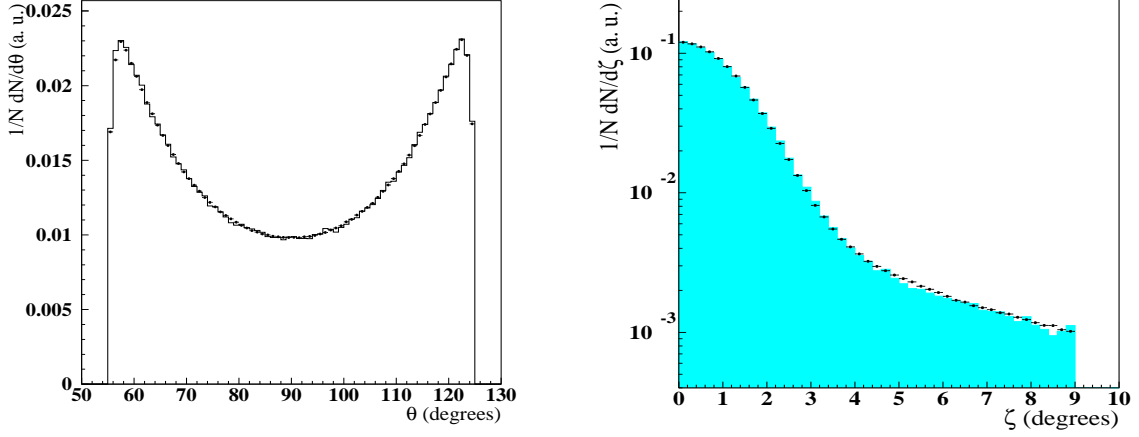


Fig. 1. Comparison between large-angle Bhabha KLOE data (points) and MC (histogram) distributions for the e^\pm polar angle θ (left) and for the acollinearity, $\zeta = |\theta_{e^+} + \theta_{e^-} - 180^\circ|$ (right), where the flight direction of the e^\pm is given by the energy deposit measured in the calorimeter. In each case, MC and data histograms are normalized to unity.

shower, in part due to the nature of the electron shower, as well as the steep e^\pm polar angle distribution.

The luminosity measured with Bhabha scattering events is often checked by using different QED processes, such as $e^+e^- \rightarrow \mu^+\mu^-$ or $e^+e^- \rightarrow \gamma\gamma$. In KLOE, the luminosity measured with $e^+e^- \rightarrow \gamma\gamma$ events differs by 0.3% with respect to Bhabha events. In CLEO-c, $e^+e^- \rightarrow \mu^+\mu^-$ events are also used and the luminosity from $\gamma\gamma$ ($\mu^+\mu^-$) is found to be 2.1% (0.6%) larger than that from Bhabha events. Fig. 2 shows the CLEO-c data for the polar angle distributions of all three processes, compared with respective MC predictions. The three QED processes are also used by the Babar experiment at the PEP-II collider, Stanford, yielding a luminosity determination of about 1% [11]. Large-angle Bhabha scattering is the normalization process primarily used by CMD-2 and SND collaborations at VEPP-2M, Novosibirsk, and by BES experiment at BEPC, Beijing.

The need of precise, namely better than 1%, and possibly redundant measurements of the collider luminosity are of utmost importance to perform accurate measurements of $e^+e^- \rightarrow \text{hadrons}$ cross sections, which are the key ingredient for evaluating the hadronic contribution to the running of α_{QED} and the muon anomaly $g - 2$.

1.2 LO cross sections and NLO corrections

As remarked in Section 1.1, the processes of interest for luminosity measurement at meson factories are Bhabha scattering and electron-positron annihilation into two photons and muon pairs. Here we present the LO formulae of the cross section of the processes $e^+e^- \rightarrow e^+e^-$ and $e^+e^- \rightarrow \gamma\gamma$, as well as the QED corrections to their cross

sections in the NLO approximation of perturbation theory. The reaction $e^+e^- \rightarrow \mu^+\mu^-$ is not addressed here because it is discussed in Section “Scan”.

1.2.1 LO cross sections

For the Bhabha scattering process

$$e^-(p_-) + e^+(p_+) \rightarrow e^-(p'_-) + e^+(p'_+) \quad (2)$$

at the Born level with pure photon exchange (see Fig. 3) the differential cross section reads as

$$\frac{d\sigma_0^{\text{Bhabha}}}{d\Omega_-} = \frac{\alpha^2}{4s} \left(\frac{3+c^2}{1-c} \right)^2 + \mathcal{O}\left(\frac{m_e^2}{s}\right), \quad (3)$$

where

$$s = (p_- + p_+)^2, \quad c = \cos \theta_-. \quad (4)$$

The angle θ_- is defined between the initial and final electron three-momenta, $d\Omega_- = d\phi_- d\theta_-$, and ϕ_- is the azimuthal angle of the outgoing electron. The small mass correction terms suppressed by the ratio m_e^2/s are negligible for the energy range and the angular acceptances here of interest.

At meson factories the Bhabha scattering cross section is largely dominated by t -channel photon exchange, followed by s - t interference and s -channel annihilation. Furthermore, Z -boson exchange contributions and other electroweak effects are suppressed at least by a factor s/M_Z^2 . In particular, for large-angle Bhabha scattering with c.m. energy $\sqrt{s} = 1$ GeV the Z boson contribution gives only about -1×10^{-5} . For $\sqrt{s} = 3$ GeV it gives -1×10^{-4} and -1×10^{-3} for $\sqrt{s} = 10$ GeV. So only at B -factories

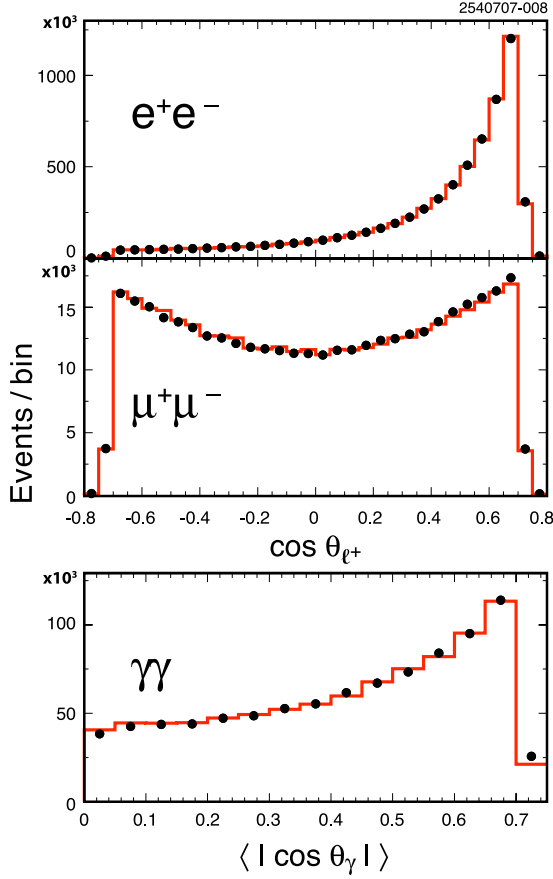


Fig. 2. Distributions of CLEO-c $\sqrt{s} = 3.774$ GeV data (circles) and MC simulations (histogram) for the polar angle of the positive lepton (upper two plots) in e^+e^- and $\mu^+\mu^-$ events, and the mean value of $|\cos \theta_\gamma|$ of the two photons in $\gamma\gamma$ events. MC histograms are normalized to the number of data events.

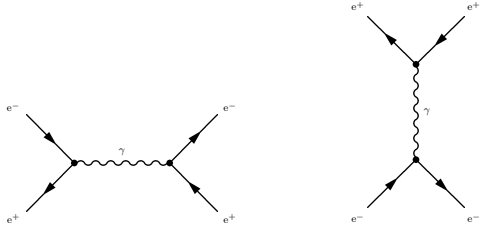


Fig. 3. LO Feynman diagrams for the Bhabha process in QED, corresponding to s -channel annihilation and t -channel scattering.

the electroweak effects should be taken into account at the tree level when aiming at a permille precision level.

The LO differential cross section of the two-photon annihilation channel (see Fig. 4)

$$e^+(p_+) + e^-(p_-) \rightarrow \gamma(q_1) + \gamma(q_2) \quad (5)$$

can be obtained by a crossing relation from the Compton scattering cross section computed by Brown and Feyn-

man [12]. It reads as follows

$$\frac{d\sigma_0^{\gamma\gamma}}{d\Omega_1} = \frac{\alpha^2}{s} \left(\frac{1+c_1^2}{1-c_1^2} \right) + \mathcal{O}\left(\frac{m_e^2}{s}\right), \quad (6)$$

where $d\Omega_1$ is an element of the first photon angular phase space. It is assumed that both the two final photons are registered in a detector, and their polar angles with respect to the initial beam directions are not small ($\theta_{1,2} \gg m_e/E$, where E is the beam energy).

1.3 NLO corrections

The complete set of NLO radiative corrections, emerging at $\mathcal{O}(\alpha)$ of perturbation theory, to Bhabha scattering and two-photon annihilation can be split into gauge-invariant subsets: QED corrections, due to emission of real photons off the charged leptons and exchange of virtual photons between them, and purely weak contributions arising from the electroweak sector of the SM.

The complete $\mathcal{O}(\alpha)$ QED corrections to Bhabha scattering are known since a long time [13, 14]. The first complete NLO prediction in the electroweak SM was performed in [15], followed by [16] and several others. At the NNLO, the leading virtual weak NNLO corrections from the top quark were derived first in [17] and are available in the fitting programs ZFITTER [18, 19] and TOPAZ0 [20, 21, 22]. The weak NNLO corrections in the Standard Model are also known for the ρ -parameter [23, 24, 25, 26, 27, 28, 29, 30, 31, 32, 33, 34, 35, 36, 37, 38, 39] and the weak mixing angle [40, 41, 42, 43, 44, 45], as well as corrections from Sudakov logarithms [46, 47, 48, 49, 50, 51, 52, 53]. Both NLO and NNLO weak effects are negligible at small energies and are not implemented yet in numerical packages for Bhabha scattering at meson factories. In pure QED, the situation is considerably different due to remarkable progress on the NNLO corrections in recent years, as emphasized and discussed in detail in Section 1.4.

As usually, the photonic corrections can be split into two parts according to their kinematics. The first part preserves the Born-like kinematics and contains the effects due to one-loop amplitudes (virtual corrections) and single soft-photon emission. Examples of Feynman diagrams giving rise to such corrections are represented in Fig. 5. The energy of a soft photon is assumed to be limited from above by ΔE , where E is the beam energy and the auxiliary parameter $\Delta \ll 1$ should be chosen in such a way that the validity of soft-photon approximation is guaranteed. The second contribution is due to hard photon emission, i.e. to single bremsstrahlung with photon energy above ΔE and corresponds to the radiative process $e^+e^- \rightarrow e^+e^-\gamma$.

Following [54, 55], the soft plus virtual (SV) correction can be cast in the form

$$\frac{d\sigma_{B+S+V}^{\text{Bhabha}}}{d\Omega_-} = \frac{d\sigma_0^{\text{Bhabha}}}{d\Omega_-} \left\{ 1 + \frac{2\alpha}{\pi} (L-1) \left[2 \ln \Delta + \frac{3}{2} \right] - \frac{8\alpha}{\pi} \ln(\text{ctg} \frac{\theta}{2}) \ln \Delta + \frac{\alpha}{\pi} K_{SV}^{\text{Bhabha}} \right\}, \quad (7)$$

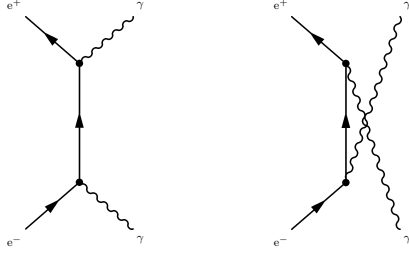


Fig. 4. LO Feynman diagrams for the process $e^+e^- \rightarrow \gamma\gamma$.

where the K -factor is given by

$$K_{SV}^{\text{Bhabha}} = -1 - 2\text{Li}_2(\sin^2 \frac{\theta}{2}) + 2\text{Li}_2(\cos^2 \frac{\theta}{2}) + \frac{1}{(3+c^2)^2} \left[\frac{\pi^2}{3} (2c^4 - 3c^3 - 15c) + 2(2c^4 - 3c^3 + 9c^2 + 3c + 21) \ln^2(\sin \frac{\theta}{2}) - 4(c^4 + c^2 - 2c) \ln^2(\cos \frac{\theta}{2}) - 4(c^3 + 4c^2 + 5c + 6) \ln^2(\text{tg} \frac{\theta}{2}) + 2(c^3 - 3c^2 + 7c - 5) \ln(\cos \frac{\theta}{2}) + 2(3c^3 + 9c^2 + 5c + 31) \ln(\sin \frac{\theta}{2}) \right], \quad (8)$$

and depends on the scattering angle, because of the contribution due to initial-final-state interference and box diagrams (see Fig. 6). It is worth noticing that the SV correction contains a leading logarithmic part enhanced by the collinear logarithm $L \equiv \ln(s/m_e^2)$.

The differential cross section of single hard bremsstrahlung

$$e^+(p_+) + e^-(p_-) \rightarrow e^+(p'_+) + e^-(p'_-) + \gamma(k)$$

for scattering angles being large compared with m_e/E reads

$$\begin{aligned} d\sigma_{\text{hard}}^{\text{Bhabha}} &= \frac{\alpha^3}{2\pi^2 s} R_{e\bar{e}\gamma} d\Gamma_{e\bar{e}\gamma}, \\ d\Gamma_{e\bar{e}\gamma} &= \frac{d^3 p'_+ d^3 p'_- d^3 k}{\varepsilon'_+ \varepsilon'_- k^0} \delta^{(4)}(p_+ + p_- - p'_+ - p'_- - k), \\ R_{e\bar{e}\gamma} &= \frac{WT}{4} - \frac{m_e^2}{(\chi'_+)^2} \left(\frac{s}{t} + \frac{t}{s} + 1 \right)^2 \\ &\quad - \frac{m_e^2}{(\chi'_-)^2} \left(\frac{s}{t_1} + \frac{t_1}{s} + 1 \right)^2 - \frac{m_e^2}{\chi_+^2} \left(\frac{s_1}{t} + \frac{t}{s_1} + 1 \right)^2 \\ &\quad - \frac{m_e^2}{\chi_-^2} \left(\frac{s_1}{t_1} + \frac{t_1}{s_1} + 1 \right)^2, \end{aligned} \quad (9)$$

where

$$\begin{aligned} W &= \frac{s}{\chi_+ \chi_-} + \frac{s_1}{\chi'_+ \chi'_-} - \frac{t_1}{\chi'_+ \chi_+} - \frac{t}{\chi'_- \chi_-} + \frac{u}{\chi'_+ \chi_-} + \frac{u_1}{\chi'_- \chi_+}, \\ T &= \frac{ss_1(s^2 + s_1^2) + tt_1(t^2 + t_1^2) + uu_1(u^2 + u_1^2)}{ss_1 tt_1}, \end{aligned}$$

and the invariants are defined as

$$\begin{aligned} s_1 &= 2p'_- p'_+, & t &= -2p_- p'_-, & t_1 &= -2p_+ p'_+, \\ u &= -2p_- p'_+, & u_1 &= -2p_+ p'_-, & \chi_{\pm} &= kp_{\pm}, & \chi'_{\pm} &= kp'_{\pm}. \end{aligned}$$

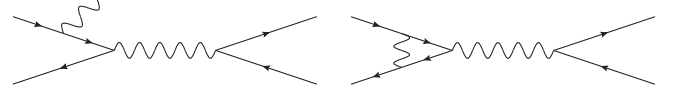


Fig. 5. Examples of Feynman diagrams for real and virtual NLO QED initial-state corrections to the s -channel contribution to the Bhabha process.

QED radiative corrections to the two-photon annihilation channel were obtained in [56, 57, 58, 59], while purely weak corrections were later computed in [60].

In the one-loop approximation the part of the differential cross section with the Born-like kinematics reads as

$$\begin{aligned} \frac{d\sigma_{B+S+V}^{\gamma\gamma}}{d\Omega_1} &= \frac{d\sigma_0^{\gamma\gamma}}{d\Omega_1} \left\{ 1 + \frac{\alpha}{\pi} \left[(L-1) \left(2 \ln \frac{\Delta\varepsilon}{\varepsilon} + \frac{3}{2} \right) + K_{SV}^{\gamma\gamma} \right] \right\}, \\ K_{SV}^{\gamma\gamma} &= \frac{\pi^2}{3} + \frac{1-c_1^2}{2(1+c_1^2)} \left[\left(1 + \frac{3}{2} \frac{1+c_1}{1-c_1} \right) \ln \frac{1-c_1}{2} + \left(1 + \frac{1-c_1}{1+c_1} + \frac{1}{2} \frac{1+c_1}{1-c_1} \right) \ln^2 \frac{1-c_1}{2} + (c_1 \rightarrow -c_1) \right], \\ c_1 &= \cos \theta_1, & \theta_1 &= \widehat{\mathbf{q}_1 \mathbf{p}_-}. \end{aligned} \quad (10)$$

In addition, the three-quantum annihilation process

$$e^+(p_+) + e^-(p_-) \rightarrow \gamma(q_1) + \gamma(q_2) + \gamma(q_3)$$

must be included, whose cross section is given by

$$\begin{aligned} d\sigma^{e^+e^- \rightarrow 3\gamma} &= \frac{\alpha^3}{8\pi^2 s} R_{3\gamma} d\Gamma_{3\gamma}, \\ R_{3\gamma} &= s \frac{\chi_3^2 + (\chi'_3)^2}{\chi_1 \chi_2 \chi'_1 \chi'_2} - 2m_e^2 \left[\frac{\chi_1^2 + \chi_2^2}{\chi_1 \chi_2 (\chi'_3)^2} + \frac{(\chi'_1)^2 + (\chi'_2)^2}{\chi'_1 \chi'_2 \chi_3^2} \right] \\ &\quad + (\text{cyclic permutations}), \\ d\Gamma_{3\gamma} &= \frac{d^3 q_1 d^3 q_2 d^3 q_3}{q_1^0 q_2^0 q_3^0} \delta^{(4)}(p_+ + p_- - q_1 - q_2 - q_3), \end{aligned} \quad (11)$$

where

$$\chi_i = q_i p_-, \quad \chi'_i = q_i p_+, \quad i = 1, 2, 3.$$

The process has to be treated as a radiative correction to the two-quantum annihilation. The energy of the third photon should exceed the auxiliary threshold ΔE . In practice, the tree photon contribution, as well as the radiative Bhabha process $e^+e^- \rightarrow e^+e^-\gamma$, should be simulated with the help of a MC event generator in order to take into account the proper experimental criteria of event selection.

In addition to the corrections discussed above, also the effect of vacuum polarization, due to the insertion of fermion loops inside the photon propagators, must be included in the precise calculation of the Bhabha scattering cross section. Its theoretical treatment, which faces the non-trivial problem of the non-perturbative contribution due to light quarks, is not discussed here since it is

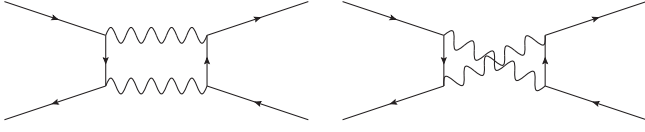


Fig. 6. Feynman diagrams for NLO QED box corrections to the s -channel contribution to the Bhabha process

addressed in detail in the Section Vacuum Polarization. However, numerical results for such correction are presented in Section 1.7 and Section 1.9.

In Fig. 7 the cross sections of the Bhabha and two photon production processes in the LO and NLO approximations are shown as a function of the c.m. energy between $\sqrt{s} \simeq 2m_\pi$ and $\sqrt{s} \simeq 10$ GeV (upper panel). The results were obtained imposing the following cuts for the Bhabha process:

$$\begin{aligned} \theta_{\pm}^{\min} &= 45^\circ & \theta_{\pm}^{\max} &= 135^\circ \\ E_{\pm}^{\min} &= 0.3\sqrt{s} & \xi_{\max} &= 10^\circ \end{aligned} \quad (12)$$

where $\theta_{\pm}^{\min, \max}$ are the angular acceptance cuts, E_{\pm}^{\min} is the minimum energy threshold for the detection of the final-state electron/positron and ξ_{\max} is the maximum e^+e^- acollinearity. For the photon pair production processes we used:

$$\begin{aligned} \theta_{\gamma}^{\min} &= 45^\circ & \theta_{\gamma}^{\max} &= 135^\circ \\ E_{\gamma}^{\min} &= 0.3\sqrt{s} & \xi_{\max} &= 10^\circ \end{aligned} \quad (13)$$

where, as in Eq. (12), $\theta_{\gamma}^{\min, \max}$ are the angular acceptance cuts, E_{γ}^{\min} is the minimum energy threshold for the detection of at least two photons and ξ_{\max} is the maximum acollinearity between the most energetic and next-to-most energetic photon.

The cross sections display the typical $1/s$ QED scaling. The relative effect of NLO corrections is shown in the upper panel. It can be seen that the NLO corrections are increasing as the c.m. energy increases, because of the growing importance of the collinear logarithm $L = \ln(s/m_e^2)$. The corrections to $e^+e^- \rightarrow \gamma\gamma$ are about one half of those to Bhabha scattering, because of the absence of final-state radiation effects in photon pair production.

1.4 NNLO Corrections to the Bhabha Scattering Cross Section

Beyond the NLO corrections discussed in the previous Section, in recent years a significant effort was devoted to the calculation of the perturbative corrections to the Bhabha process at the NNLO in QED.

The calculation of the full NNLO corrections to the Bhabha scattering cross section requires three types of ingredients: *i*) the two-loop matrix elements for the $e^+e^- \rightarrow e^+e^-$ process; *ii*) the one-loop matrix elements for the $e^+e^- \rightarrow e^+e^- \gamma$ process, both in the case in which the

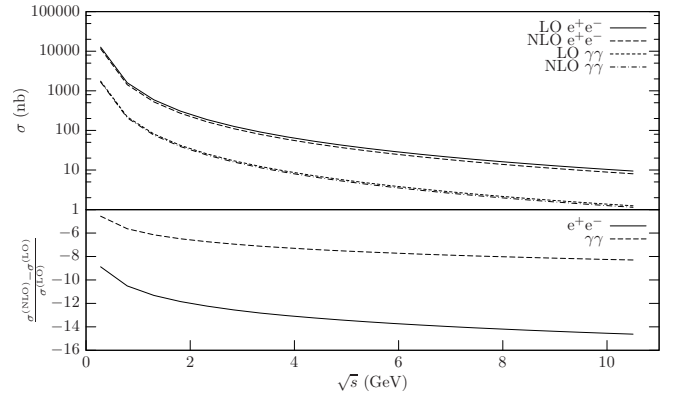


Fig. 7. Cross sections of the processes $e^+e^- \rightarrow e^+e^-$ and $e^+e^- \rightarrow \gamma\gamma$ in the LO and NLO approximations, as a function of the c.m. energy at meson factories (upper panel). In the lower panel, the relative contribution due to NLO QED corrections to the two processes is shown.

additional photon is soft or hard; *iii*) the tree-level matrix elements for $e^+e^- \rightarrow e^+e^- \gamma\gamma$, with two soft, two hard or one soft and one hard photons. Also the process $e^+e^- \rightarrow e^+e^- e^+e^-$, with one of the two e^+e^- pairs to be considered as undetected contributes to the Bhabha signature at NNLO, because the data taking at meson factories typically requires the presence of at least two tracks in the detector. Dependent on the kinematics, other final states like e.g. $e^+e^- \mu^+ \mu^-$ or those with hadrons are also possible.

The advent of new calculational techniques and a deeper understanding of the IR structure of unbroken theories, such as QED or QCD, made the calculation of the complete set of two-loop QED corrections possible. The history of this calculation will be presented in Section 1.4.1.

We consider then the one-loop matrix elements with three particles in the final state. The diagrams involving the emission of a soft photon are known and they were included in the calculations of the two-loop matrix elements, in order to remove the IR soft divergencies. However, although the contributions due to a hard-collinear photon are taken into account in logarithmic accuracy by the MC generators, a full calculation of the diagrams involving a hard-photon in a general phase-space configuration is still missing. In Section 1.4.2, we will comment on the possible strategies which can be adopted in order to calculate these corrections.

As a general comment, it must be noticed that the fixed-order corrections calculated through NNLO calculations are taken into account at the leading logarithmic (LL) level into the MC generators, which include, as discussed in Section 1.5 and Section 1.6, the logarithmically enhanced contributions of soft and collinear photons at all orders in perturbation theory.

Concerning the tree level graphs with four particles in the final state, the production of a soft e^+e^- pair was addressed in the literature, but only with logarithmic accuracy, and it is included in the two-loop calculation (see Section 1.4.1. New results obtained during the workshop

about lepton and hadron pair corrections, which are presently neglected into the available Bhabha codes, are presented in Section 1.4.3.

1.4.1 Virtual corrections for the $e^+e^- \rightarrow e^+e^-$ process

The calculation of the virtual two-loop QED corrections to the Bhabha scattering differential cross section was carried out in the last 10 years. This calculation was made possible by an improvement of the techniques employed in the evaluation of multiloop Feynman diagrams. An essential tool used to manage the calculation is the Laporta algorithm [61, 62, 63, 64], which allows to reduce a generic combination of dimensionally-regularized scalar integrals to a combination of a small set of independent integrals called the “Master Integrals” (MIs) of the problem under consideration. The calculation of the MIs is then pursued by means of a variety of methods. Particularly important are the differential equations method [65, 66, 67, 68, 69, 70, 71] and the Mellin-Barnes techniques [72, 73, 74, 75, 76, 77, 78, 79, 80, 81]. Both methods proved to be very useful in the evaluation of virtual corrections to Bhabha scattering since they are especially effective in problems with a small number of different kinematical parameters. They both allow one to obtain an analytic expression for the integrals, which must be written in terms of a suitable functional basis. A basis which was extensively employed in the calculation of multiloop Feynman diagrams of the type discussed here is represented by the Harmonic Polylogarithms [82, 83, 84, 85, 86, 87, 88, 89, 90] and their generalizations. Another fundamental achievement which allowed to complete the calculation of the QED two-loop corrections was an improved understanding of the IR structure of QED. In particular, the relation between the collinear logarithms in which the electron mass m_e plays the role of a natural cut-off and the corresponding poles in the dimensionally regularized massless theory was extensively investigated in [91, 92, 93, 94].

A first complete diagrammatic calculation of the two-loop QED virtual corrections to Bhabha scattering can be found in [95]. However, this result was obtained in the fully massless approximation ($m_e = 0$), by employing dimensional regularization (DR) to regulate both soft and collinear divergencies. Today, the complete set of two-loop corrections to Bhabha scattering in pure QED have been evaluated using m_e as a collinear regulator, as required in order to include these fixed-order calculations in available Monte Carlo event generators. The Feynman diagrams involved in the calculation can be divided in three gauge independent sets: *i*) diagrams without fermion loops (“photonic” diagrams), *ii*) diagrams involving a closed electron loop, and *iii*) diagrams involving a closed loop of hadrons or a fermion heavier than the electron. Some of the diagrams belonging to the aforementioned sets are shown in Figs. 8–13. These three sets are discussed in more details below.

A large part of the NNLO photonic corrections can be evaluated in a closed analytic form, retaining the full dependence on m_e [96], by using the Laporta algorithm for the reduction of the Feynman diagrams to a combination of MIs, and then the differential equations method for the MIs analytic evaluation. With this technique it is possible to calculate, for instance, the NNLO corrections to the form factors [97, 98]. However, a calculation of the two-loop photonic boxes retaining the full dependence on m_e seems to be beyond the reach of this method. This is due to the fact that the number of Master Integrals belonging to the same topology is, in some cases, large. Therefore, one must solve analytically large systems of first-order ordinary linear differential equations; this is not possible in general. Alternatively, in order to calculate the different MIs involved, one could use the Mellin-Barnes techniques, as shown in [78, 79, 98, 99, 100, 101], or a combination of both methods. The calculation is very complicated and a full result is not yet available¹. However, the full dependence on m_e is not phenomenologically relevant. In fact, the physical problem exhibits a well defined mass hierarchy. The mass of the electron is always very small compared to the other kinematic invariants and it can be safely neglected everywhere, with the exception of the terms in which it acts as a collinear regulator. The ratio of the photonic NNLO corrections to the Born cross section is the following²

$$\frac{d\sigma^{(2,\text{PH})}}{d\sigma^{(\text{Born})}} = \frac{\alpha^2}{\pi^2} \sum_{i=0}^2 \delta^{(\text{PH},i)} L_e^i + \mathcal{O}\left(\frac{m_e^2}{s}, \frac{m_e^2}{t}\right), \quad (14)$$

where $L_e = \ln(s/m_e^2)$ and where the coefficients $\delta^{(\text{PH},i)}$ are functions of the scattering angle θ . The approximation given by Eq. (14) is sufficient for a phenomenological description of the process³. The coefficients of the double and single collinear logarithm in Eq. (14), $\delta^{(\text{PH},2)}$ and $\delta^{(\text{PH},1)}$, were obtained in [102, 103]. However, the precision required for luminosity measurements at e^+e^- colliders demands the calculation of the non-logarithmic coefficient, $\delta^{(\text{PH},0)}$. The latter was obtained in [91, 92] by reconstructing the differential cross section in the $s \gg m_e^2 \neq 0$ limit from the dimensionally regularized massless approximation [95]. The main idea of the method developed in [91, 92] is outlined below. As far as the leading term in the small electron mass expansion is considered, the dif-

¹ For the planar double box diagrams, all the MI integrals are known [99] for small m_e , while the MIs for the non-planar double box diagrams are not completed.

² Infrared logarithms have been omitted in Eq. (14) and following ones, because they disappear when summing up the contribution of hard photons and inclusive photon energy conditions are considered.

³ It can be shown that the terms suppressed by a positive power of m_e^2/s do not play any phenomenological role already at very low c.m. energies, $\sqrt{s} \sim 10$ MeV. Moreover, the terms m_e^2/t (or m_e^2/u) become important in the extremely forward (backward) region, unreachable for the experimental set ups.

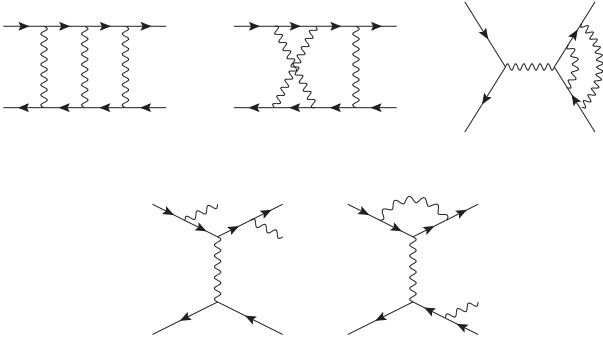


Fig. 8. Some of the diagrams belonging to the class of the “photonic” NNLO corrections to the Bhabha scattering differential cross section. The additional photons in the final state are soft.

ference between the massive and the dimensionally regularized massless Bhabha scattering can be viewed as a difference between two regularization schemes for the infrared divergences. With the known massless two-loop result at hand, the calculation of the massive one is reduced to constructing the *infrared matching* term which relates the two above mentioned regularization schemes. To perform the matching an auxiliary amplitude is constructed, which has the same structure of the infrared singularities but is sufficiently simple to be evaluated at least in leading order in the small mass expansion. A particular form of the auxiliary amplitude is dictated by the general theory of infrared singularities in QED and involves the exponent of the one-loop correction as well as the two-loop corrections to the *logarithm* of the electron form factor. The difference between the full and the auxiliary amplitudes is infrared finite. It can be evaluated by using dimensional regularization for each amplitude and then taking the limit of four space-time dimensions. The infrared divergences, which induce the asymptotic dependence of the virtual corrections on the electron and photon masses, are absorbed into the auxiliary amplitude while the technically most nontrivial calculation of the full amplitude is performed in the massless approximation. The matching of the massive and massless results is then necessary only for the auxiliary amplitude and it is straightforward. Thus the two-loop massless result for the scattering amplitude along with the two-loop massive electron form factor [104] are sufficient to obtain the two-loop photonic correction to the differential cross section in the small electron mass limit.

A method based on a similar principle was subsequently developed in [93, 94]; the authors of [94] confirmed the result of [91, 92] for the NNLO photonic corrections to the Bhabha scattering differential cross section.

$$\frac{d\sigma^{(2,EL)}}{d\sigma^{(Born)}} = \frac{\alpha^2}{\pi^2} \sum_{i=0}^3 \delta^{(EL,i)} L_e^i + \mathcal{O}\left(\frac{m_e^2}{s}, \frac{m_e^2}{t}\right). \quad (15)$$

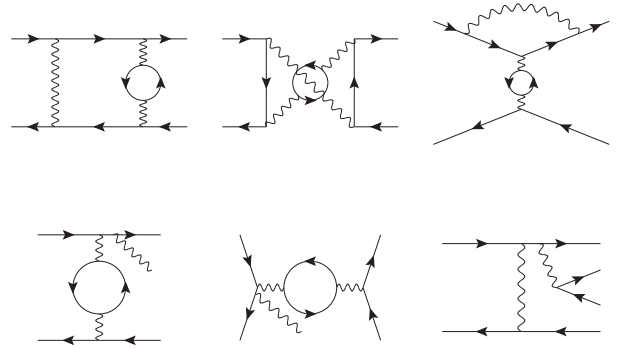


Fig. 9. Some of the diagrams belonging to the class of the “electron loop” NNLO corrections. The additional photons or electron-positron pair in the final state are soft.

Electron Loop Corrections

The NNLO electron loop corrections arise from the interference of two-loop Feynman diagrams with the tree-level amplitude as well as from the interference of one-loop diagrams, as long as one of the diagrams contributing to each term involves a closed electron loop. This set of corrections presents a single two-loop box topology, and it is therefore technically less challenging to evaluate with respect to the photonic correction set. The calculation of the electron loop corrections was completed a few years ago [105, 106, 107, 108]; the final result retains the full dependence of the differential cross section on the electron mass m_e . The MIs involved in the calculation were identified by means of the Laporta algorithm and evaluated with the differential equation method. As expected, after UV renormalization the differential cross section presented only residual IR poles which were removed by adding the contribution of the soft photon emission diagrams. The resulting NNLO differential cross section could be conveniently written in terms of 1- and 2-dimensional Harmonic Polylogarithms (HPLs) of maximum weight three. Expanding the cross section in the limit $s, |t| \gg m_e^2$, the ratio of the NNLO corrections to the Born cross section can be written as in Eq. (14):

$$\frac{d\sigma^{(2,EL)}}{d\sigma^{(Born)}} = \frac{\alpha^2}{\pi^2} \sum_{i=0}^3 \delta^{(EL,i)} L_e^i + \mathcal{O}\left(\frac{m_e^2}{s}, \frac{m_e^2}{t}\right). \quad (16)$$

Note that the series now starts with a cubic collinear logarithm. This logarithm appears, with an opposite sign, in the corrections due to the production of an electron-positron pair (the soft-pair production was considered in [109]). When the two contributions are considered together in the full NNLO, the cubic collinear logarithms cancel. Therefore, the physical cross section includes at most a double logarithm, as in Eq. (14).

The explicit expression of all the coefficients $\delta^{(EL,i)}$, obtained by expanding the results of [105, 106, 107] was confirmed by two different groups [94, 108]. In [94] the small electron mass expansion was performed within the soft-collinear effective theory (SCET) framework, while the analysis in [108] employed the asymptotic expansion of

the Master Integrals.

Heavy-Flavor and Hadronic Corrections

Finally, we consider the corrections originating from two-loop Feynman diagrams involving a heavy flavor fermion loop⁴. Since this set of corrections involves one more mass scale with respect to the corrections analyzed in the previous sections, a direct diagrammatic calculation is in principle a more challenging task. Recently, in [94] the authors applied their technique based on SCET to Bhabha scattering and obtained the heavy flavor NNLO corrections in the limit in which $s, |t|, |u| \gg m_f^2 \gg m_e^2$, where m_f^2 is the mass of the heavy fermion running in the loop. Their result was very soon confirmed in [108] by means of a method based on the asymptotic expansion of Mellin Barnes representation of the Master Integrals involved in the calculation. However, the results obtained in the approximation $s, |t|, |u| \gg m_f^2 \gg m_e^2$ cannot be applied to the case in which the $\sqrt{s} < m_f$ (as in the case of a tau loop at $\sqrt{s} \sim 1$ GeV), and they apply only to a relatively narrow angular region perpendicular to the beam direction when \sqrt{s} is not very much larger than m_f (as in the case of top-quark loops at ILC). It was therefore necessary to calculate the heavy flavor corrections to Bhabha scattering assuming only that the electron mass is much smaller than the other scales in the process, but retaining the full dependence on the heavy mass, $s, |t|, |u|, m_f^2 \gg m_e^2$.

The calculation was carried out in two different ways: in [110, 111] it was done analytically, while in [112, 113] it was done numerically with the dispersion relations.

The technical problem of the diagrammatic calculation of Feynman integrals with four scales can be simplified by considering carefully, once more, the structure of the collinear singularities of the heavy-flavor corrections. The ratio of the NNLO heavy flavor corrections to the Born cross section is given by

$$\frac{d\sigma^{(2, \text{HF})}}{d\sigma^{(\text{Born})}} = \frac{\alpha^2}{\pi^2} \sum_{i=0}^1 \delta^{(\text{HF}, i)} L_e^i + \mathcal{O}\left(\frac{m_e^2}{s}, \frac{m_e^2}{t}\right), \quad (17)$$

where now the coefficients $\delta^{(i)}$ are functions of the scattering angle θ and, in general, of the mass of the heavy fermions involved in the virtual corrections. It is possible to prove that, in a physical gauge, all the collinear singularities factorize and can be absorbed in the external field renormalization [114]. This observation has two consequences in the case at hand. The first one is that box diagrams are free of collinear divergencies in a physical gauge; since the sum of all boxes forms a gauge independent block, it can be concluded that the sum of all box diagrams is free of collinear divergencies in any gauge. The second consequence is that the single collinear logarithm in Eq. (17) arises from vertex corrections only. Moreover, if one chooses on-shell UV renormalization conditions, the irreducible two-loop vertex graphs are free

⁴ Here by “heavy flavor” we mean a muon or a tau-lepton, as well as an heavy quark, like the top, the b - or the c -quark, depending on the c.m. energy range that we are considering.

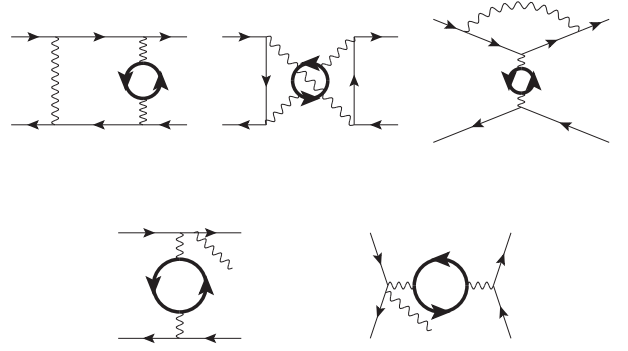


Fig. 10. Some of the diagrams belonging to the class of the “heavy fermion” NNLO corrections. The additional photons in the final state are soft.

of collinear singularities. Therefore, among all the two-loop diagrams contributing to the NNLO heavy flavor corrections to Bhabha scattering, only the reducible vertex corrections are logarithmically divergent in the $m_e \rightarrow 0$ limit⁵. The latter are easily evaluated even if they depend on two different masses. By exploiting these two facts, one can obtain the NNLO heavy-flavor corrections to the Bhabha scattering differential cross section assuming only that $s, |t|, |u|, m_f^2 \gg m_e^2$. In particular, one can set $m_e = 0$ from the start in all the two-loop diagrams with the exception of the reducible ones. This procedure allows one to effectively eliminate a mass scale from the two-loop boxes, so that these graphs can be evaluated with the techniques already employed in the diagrammatic calculation of the electron loop corrections⁶. In the case in which the heavy flavor fermion is a quark, it is straightforward to modify the calculation of the two-loop self-energy diagrams to obtain the mixed QED-QCD corrections to Bhabha scattering [111].

An alternative approach to the calculation of the heavy flavor corrections to Bhabha scattering, is based on dispersion relations. This method also applies to hadronic corrections. The hadronic and heavy-fermion corrections to the Bhabha-scattering cross section can be obtained by appropriately inserting the renormalized irreducible photon vacuum-polarization function Π in the photon propagator:

$$\frac{g_{\mu\nu}}{q^2 + i\delta} \rightarrow \frac{g_{\mu\alpha}}{q^2 + i\delta} (q^2 g^{\alpha\beta} - q^\alpha q^\beta) \Pi(q^2) \frac{g_{\beta\nu}}{q^2 + i\delta}. \quad (18)$$

The vacuum polarization Π can be represented by a once-subtracted dispersion integral [1],

$$\Pi(q^2) = -\frac{q^2}{\pi} \int_{4M^2}^{\infty} dz \frac{\text{Im} \Pi(z)}{z} \frac{1}{q^2 - z + i\delta}. \quad (19)$$

⁵ Additional collinear logarithms arise also from the interference of one-loop diagrams in which at least one vertex is present.

⁶ The necessary MIs can be found in [111, 115, 116, 117].

The contributions to Π then may be determined from a (properly normalized) production cross-section by the optical theorem [118],

$$\text{Im } \Pi_{\text{had}}(z) = -\frac{\alpha}{3} R_{\text{had}}(z). \quad (20)$$

In this way, the hadronic vacuum polarization may be obtained from the experimental data for R_{had} :

$$R_{\text{had}}(z) = \frac{\sigma(\{e^+e^- \rightarrow \gamma^* \rightarrow \text{hadrons}\}; z)}{(4\pi\alpha^2)/(3z)}. \quad (21)$$

In the low-energy region the inclusive experimental data may be used [119, 120]. Around a narrow hadronic resonance with mass M_{res} and width $\Gamma_{\text{res}}^{e^+e^-}$ one may use the relation

$$R_{\text{res}}(z) = \frac{9\pi}{\alpha^2} M_{\text{res}} \Gamma_{\text{res}}^{e^+e^-} \delta(z - M_{\text{res}}^2), \quad (22)$$

and in the remaining regions the perturbative QCD prediction [121]. Contributions to Π arising from leptons and heavy quarks with mass m_f , charge Q_f and color C_f can be computed directly in perturbation theory:

$$R_f(z; m_f) = Q_f^2 C_f \left(1 + 2 \frac{m_f^2}{z}\right) \sqrt{1 - 4 \frac{m_f^2}{z}}. \quad (23)$$

As a result of the above, the massless photon propagator gets replaced by a massive propagator, whose effective mass z is subsequently integrated over:

$$\frac{g_{\mu\nu}}{q^2 + i\delta} \rightarrow \frac{\alpha}{3\pi} \int_{4M^2}^{\infty} \frac{dz R(z)}{z(q^2 - z + i\delta)} \left(g_{\mu\nu} - \frac{q_\mu q_\nu}{q^2 + i\delta}\right). \quad (24)$$

For self-energy corrections to Bhabha scattering at one-loop order, the dispersion approach was first employed in [122]. Two-loop applications of this technique, prior to Bhabha scattering, are the evaluation of the hadronic vertex correction [123] and of two-loop hadronic corrections to the lifetime of the muon [124].

The fermionic and hadronic corrections to Bhabha scattering at one-loop accuracy come only from the self-energy diagram; see for details Section 5 “Vacuum polarization”. At two-loop level, there are reducible and irreducible self-energy contributions, vertices and boxes. The reducible corrections are easily treated. For the evaluation of the irreducible two-loop diagrams, it is advantageous that they are one-loop diagrams with self-energy insertions, because the application of the dispersion technique as described here is possible.

The kernel function for the irreducible two-loop vertex was derived in [123] and verified in e.g. [113], and the three kernel functions for the two-loop box functions were first obtained in [125, 112, 113] and verified in [126]. A complete collection of all the relevant formulae may be found in [113], and the corresponding Fortran code bhhbnnloh is publicly available, see the webpage [127] at <http://www-zeuthen.desy.de/theory/research/bhabha/>. In

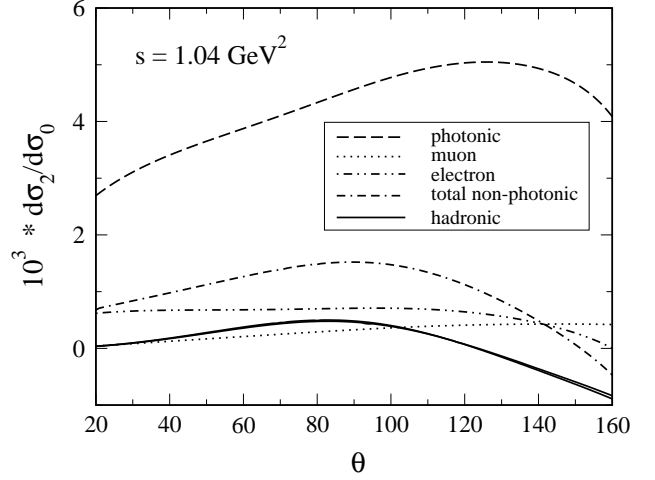


Fig. 11. Two-loop corrections to Bhabha scattering at $\sqrt{s} = 1.02$ GeV, normalized to the QED tree-level cross section, as a function of the electron polar angle. No cuts. The parameterization of R_{had} due to [128] and [119, 120, 121] are very close to each other.

[113], the dependence of the various heavy-fermion NNLO corrections on $\ln(s/m_f^2)$ for $s, |t|, |u| \gg m_f^2$ was studied. The irreducible vertex behaves (before a combination with real pair emission terms) like $\ln^3(s/m_f^2)$ [123], while the sum of the various infrared divergent diagrams as a whole behaves like $\ln(s/m_f^2) \ln(s/m_e^2)$. This is in accordance with (17), but the limit plays no effective role at the energies studied here.

As a result of recent years efforts, we have now for all the non-photonic virtual two-loop contributions at least two completely independent calculations. The net result, as a ratio of the NNLO corrections to the Born cross section in per mille, is shown in Figure 11 for KLOE and in Figure 12 for BABAR/BELLE. While the non-photonic corrections stay at 1 per mille or less for KLOE, they reach a few per mille at the BABAR/BELLE energy range. The photonic NNLO corrections amount to some per mille, both at Φ and B factories. However, as already emphasized, the bulk of both photonic and non-photonic corrections is incorporated into the generators used by the experimental collaborations. Hence, the consistent comparison between the results of NNLO calculations and the MC predictions at the same perturbative level allows to settle the theoretical accuracy of the luminosity tools, as discussed quantitatively in Section 1.9.

1.4.2 Fixed-Order calculation of the Hard Photon Emission at One Loop

The one-loop matrix element for the process $e^+e^- \rightarrow e^+e^-\gamma$ is one of the contributions to the complete set of NNLO corrections to Bhabha scattering. Its evaluation requires the non-trivial computation of one-loop tensor integrals associated to pentagon-diagrams.

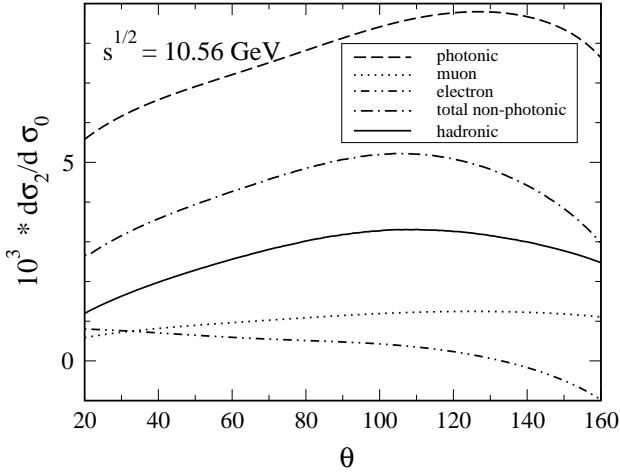


Fig. 12. Two-loop corrections to Bhabha scattering at $\sqrt{s} = 10.56$ GeV, normalized to the QED tree-level cross section, as a function of the electron polar angle. No cuts. The parameterization of R_{had} is due to [128].

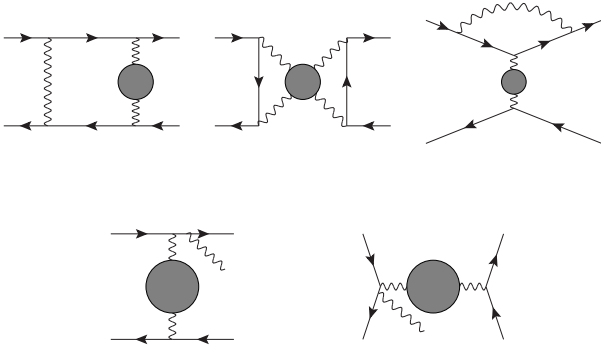


Fig. 13. Some of the diagrams belonging to the class of the “hadronic” corrections. The additional photons in the final state are soft.

According to the standard Passarino-Veltman (PV) approach [129], one-loop tensor integrals can be expressed in terms of scalar integrals, called Master Integrals (MIs), with trivial numerators that are independent of the loop variable, each multiplied by a Lorentz structure depending only on combinations of the external momenta and the metric tensor. The achievement of the complete PV-reduction amounts to solve a non-trivial system of equations. TR: The next statement is not clear to me. I try to modify, please check if it is ok with you. Due to its size, it is reasonable replacing the analytic techniques by numerical tools. It is difficult to implement the PV-reduction numerically, since it gives rise to Gram determinants. The latters naturally arise in the procedure of inverting a system and they can vanish in special phase-space points. This fact requires a proper modification of the reduction algorithm [130,131,132,133,134,135,136]. A viable solution for the complete algebraic reduction of tensor-pentagon (and tensor-hexagon) integrals was formulated

in [137,138,139], by exploiting the algebra of signed minors [140]. In this approach, the cancelation of powers of inverse Gram determinants was performed recently in [141,142].

The computation of the one-loop 5-point amplitude $e^+e^- \rightarrow e^+e^-\gamma$ can be alternatively performed by using generalized-unitarity cutting rules (see [143] for a detailed compilation of references). In the following, we propose two ways to achieve the result, respectively *via* an analytical and a semi-numerical method. The application of generalized cutting-rules as an on-shell method of calculation is based on two fundamental properties of scattering amplitudes: *i*) analyticity, according to which any amplitude is determined by its own singularity structure [144,145,146,118,147]; *ii*) and unitarity, according to which the residues at the singularities are determined by products of simpler amplitudes. Turning these properties into a tool for computing scattering amplitudes is possible because of the underlying representation of the amplitude in terms of Feynman integrals and their PV-reduction, which grants the existence of a representation of any one-loop amplitudes as linear combination of MIs, each multiplied by a rational coefficient. In the case of $e^+e^- \rightarrow e^+e^-\gamma$, pentagon-integrals should be ultimately may be expressed, though PV-reduction, to a linear combination of 17 MIs (including 3 boxes, 8 triangles, 5 bubbles, and 1 tadpole). Since the required MIs are analytically known [148,149,150,138,132,151,152], the determination of their coefficients is what is needed for reconstructing the amplitude as a whole. To this aim, one may use the Mathematica program hexagon [141,142]. Also, matching the generalized cuts of the amplitude against the cuts of the MIs provides an efficient way to extract their (rational) coefficients out of the amplitude itself. In general, the fulfillment of multiple-cut conditions requires loop momenta with complex components. The effect of the cut-conditions is to freeze some of its components, when not all, according to the number of the cuts. With the quadruple-cut [153] the loop momentum is completely frozen, yielding the algebraic determination of the coefficients of n -point functions with $n \geq 4$. In cases where fewer than four denominators are cut, like triple-cut [154,155,156], double-cut [157,158,159,160,161,155], and single-cut [162], the loop momentum is not frozen: the free-components are left over as phase-space integration variables.

For each multiple-cut, the evaluation of the phase-space integral would generate, in general, logarithms and a non-logarithmic term. The coefficient of a given n -point MI finally appears in the non-logarithmic term of the corresponding n -particle cut, where all the internal line are on-shell (while the logarithms correspond to the cuts of higher-point MIs which share that same cut). Therefore all the coefficients of MIs can be determined in a *top-down* algorithm, starting from the quadruple-cuts for the extraction of the 4-point coefficients, and following with the triple-, double-, and single-cuts, for the coefficients of 3-, 2- and 1-point, respectively. The coefficient of an n -point MI ($n \geq 2$) can be also obtained by specializing to

the case at hands the generating formulas given in [163] for general one-loop amplitudes.

Instead of the analytic evaluation of the multiple-cut phase-space integrals, it is worth considering the feasibility of computing the process $e^+e^- \rightarrow e^+e^-\gamma$ with a seminumerical technique by-now known as OPP-reduction [164, 165], based on the decomposition of the numerator of any one-loop integrand in terms of its denominators [166, 167, 168, 169]. Within this approach, the coefficients of the MIs can be found simply by solving a system of numerical equations, and avoiding any explicit integration. The OPP-reduction algorithm exploits the polynomial structures of the integrand when evaluated at values of the loop-momentum fulfilling multiple cut-conditions: *i*) for each n -point MI, one considers the n -particle cut obtained by setting all the propagating lines on-shell; *ii*) such a cut is associated to a polynomial in terms of the free components of the loop-momentum, which corresponds to the numerator of the integrand evaluated at the solution of the on-shell conditions; *iii*) the constant-term of that polynomial is the coefficient of the MI.

Hence, the difficult task of evaluating one-loop Feynman integrals is reduced to the much simpler problem of polynomial fitting, recently optimized by using a projection-technique based on the Discrete Fourier Transform [170].

In general the result of a dimensional-regulated amplitude in the 4-dimensional limit, being $D (= 4 - 2\epsilon)$ the regulating parameter, is expected to contain (poly)logarithms, often referred to as the cut-constructible term, and a pure rational term. In a remarkable over-emphasized? paper [171] which completed the OPP-method, the rising of the rational term was attributed to two potential sources (of UV-divergent integrals): one, defined R_1 , due to the D -dimensional completion of the 4-dimensional contribution of the numerator; a second one, called R_2 , due to the (-2ϵ) -dimensional algebra of Dirac-matrices. Therefore in the OPP-approach the calculation of the one-loop amplitude $e^+e^- \rightarrow e^+e^-\gamma$ can proceed through two computational stages:

1. the coefficients of the MIs that are responsible both for the cut-constructible and for the R_1 -rational terms can be determined by applying the OPP-reduction discussed above [164, 165, 170];
2. the R_2 -rational term can be computed by using additional tree-level-like diagrammatic rules, very much resembling the computation of the counter terms needed for the renormalization of UV-divergencies [171].

The numerical influence of the radiative loop diagrams, including the pentagon diagrams, is expected to be not particularly large. However, the calculation of such corrections would greatly help to assess the physical precision of existing programs.

1.4.3 Pair Corrections

As was mentioned in the part on virtual heavy flavor and hadronic corrections of Section 1.4.1, these virtual corrections have to be combined with real corrections in order to get physically sensible results. The virtual NNLO

electronic, muonic, pion corrections have to be combined with the emission of real electron, muon, pion pairs, respectively. The real pair production cross sections are finite, but cut dependent. As was first explicitly shown for Bhabha scattering in [109] for electron pairs, and also discussed in [113], there appear exact cancellations of terms of the order $\ln^3(s/m_e^2)$ or $\ln^3(s/m_f^2)$, so that the leading terms are at most of order $\ln^2(s/m_e^2), \ln^2(s/m_f^2)$.

In Table 1 we show sample NNLO contributions with typical kinematical cuts for KLOE and Babar/Belle energies. Besides contributions from unresolved pair emissions σ_{pairs} , we also add unresolved real hard photon emission contributions σ_{hard} . The corrections σ_{pairs} from fermions have been calculated with the Fortran package HELAC-PHEGAS [172, 173, 174, 175], the real pion corrections with PHOKHARA [176, 177], the NNLO hard photonic corrections σ_h with a program from Czyz etc., please quote [?]. The latter depend, technically, on the soft photon cut-off $E_\gamma^{\min} = \omega$. After adding up with σ_{v+s} , the sum of the two σ_{v+s+h} is independent of that; in fact we use here $\omega/E_{beam} = 10^{-4}$. The σ_{v+s} is determined with an updated version of the Fortran package bhhnnlohf [113, 127] in order to cover also pion pair corrections. Cuts, which tend to single out Bhabha events, have been applied in Table 1; for the Φ factory KLOE/DAΦNE (Frascati):

- $\sqrt{s} = 1.02 \text{ GeV}$
- $E_{min} = 0.4 \text{ GeV}$
- $55^\circ < \theta_\pm < 125^\circ$
- $\xi_{max} = 9^\circ$,

and for the B -factories BABAR/PEP-II (SLAC) and BELLE/KEKB (KEK):

- $\sqrt{s} = 10.56 \text{ GeV}$
- $|\cos(\theta_\pm)| < 0.7$ and $|\cos(\theta_+)| < 0.65$ or $|\cos(\theta_-)| < 0.65$
- $|\mathbf{p}_+|/E_{beam} > 0.75$ and $|\mathbf{p}_-|/E_{beam} > 0.5$ or $|\mathbf{p}_-|/E_{beam} > 0.75$ and $|\mathbf{p}_+|/E_{beam} > 0.5$
- $\xi_{max}^{3d} = 30^\circ$.

Here it is E_{min} the energy threshold for the final state electron/positron, θ_\pm are the electron/positron polar angles and ξ_{max} is the maximum allowed polar angle acollinearity:

$$\xi = |\theta_+ + \theta_- - 180^\circ|, \quad (25)$$

and ξ_{max}^{3d} is the maximum allowed three dimensional acollinearity:

$$\xi^{3d} = \left| \arccos \left(\frac{\mathbf{p}_+ \cdot \mathbf{p}_-}{(|\mathbf{p}_-||\mathbf{p}_+|)} \right) \times \frac{180^\circ}{\pi} - 180^\circ \right|. \quad (26)$$

For $e^+e^- \rightarrow e^+e^-\mu^+\mu^-$, cuts are applied only to the e^+e^- pair. In the case of $e^+e^- \rightarrow e^+e^-e^+e^-$, all possible $e^\pm e^\mp$ combinations are checked and if at least one pair fulfils the cuts the event is accepted.

At KLOE, the electron pair corrections contribute at about 5×10^{-4} , and at BABAR/BELLE at about 2.5×10^{-3} , while all the other cases studied are even smaller. Like in small-angle Bhabha scattering at LEP/SLC, the

Table 1. The NNLO corrections to the Bhabha scattering Born cross section σ_B : virtual corrections σ_v , soft and hard real photon emissions σ_s, σ_h , and pair emission contributions σ_{pairs} ; all cross sections in nanobarns with an angular acceptance cut $|\cos\theta| < 0.7$.

Electron pair corrections					
	σ_B	σ_h	σ_{v+s}	σ_{v+s+h}	σ_{pairs}
KLOE	529.055	8.632	-11.564	-2.932	0.271
BABAR	6.748	0.296	-0.271	0.025	0.017
Muon pair corrections					
	σ_B	σ_h	σ_{v+s}	σ_{v+s+h}	σ_{pairs}
KLOE	529.055	1.357	-1.598	-0.242	–
BABAR	6.748	0.112	-0.114	-0.0022	0.0005
Tau pair corrections					
	σ_B	σ_h	σ_{v+s}	σ_{v+s+h}	σ_{pairs}
KLOE	529.055	0.018	-0.022	-0.003	–
BABAR	6.748	0.019	-0.020	-0.0007	–
Pion pair corrections					
	σ_B	σ_h	σ_{v+s}	σ_{v+s+h}	σ_{pairs}
KLOE	529.055	1.066	-1.252	-0.186	–
BABAR	6.748	0.075	-0.078	-0.0026	0.0003

pair corrections [178] are largely dominated by the electron pair contribution. Check that the numbers are correct.

1.5 Multiple photon effects and matching with NLO corrections

1.5.1 Universal methods for leading logarithmic corrections

From inspection of Eq. (7) and Eq.(10) for the SV NLO QED corrections to the cross section of the Bhabha scattering and $e^+e^- \rightarrow \gamma\gamma$ process, it can be seen that large logarithms $L = \ln(s/m_e^2)$, due to collinear photon emission, are present. Similar large logarithmic terms arise after integration of the hard photon contributions from the kinematical domains of photon emission at small angles with respect to charged particles. For the energy range of meson factories, the logarithm is large numerically, i.e. $L \gtrsim 15$ and the corresponding terms give the bulk of the total radiative correction. These contributions represent also the dominant part of the NNLO effects discussed in Section 1.4. Therefore, the logarithmically enhanced contributions due to emission of soft and collinear photons must be taken into account at all orders in perturbation theory, to achieve the required theoretical accuracy.

The methods for the calculation of higher-order (HO) QED corrections on the grounds of the generators employed nowadays at flavour factories were already used, widely and successfully, in the 90s at LEP/SLC for electroweak tests of the SM. They have been adopted for the calculation of both the small-angle Bhabha scattering cross section (necessary for the high-precision luminosity measurement) and Z -boson observables. Hence, the theory accounting for the control of HO QED corrections at meson factories can be considered particularly robust, having passed the very stringent tests of LEP/SLC era.

The most popular and standard approach to keep under control multiple photon effects are the QED Structure Function (SF) method [179, 180, 181, 182], and Yennie-Frautschi-Suura (YFS) exponentiation [183]. The former is used in all the version of the generator BabaYaga [184, 185, 186] and MCGPJ [187] (albeit according to different realizations), while the latter is the theoretical recipe adopted in BHWIDE [188]. Actually, analytical QED SFs $D(x, Q^2)$, valid in the strictly collinear approximation, are implemented in MCGPJ, whereas BabaYaga is based on a MC Parton Shower (PS) algorithm to reconstruct $D(x, Q^2)$ numerically.

The Structure Function approach

Let us consider, for definiteness, the annihilation process $e^-e^+ \rightarrow X$, where X is some given final state, and $\sigma_0(s)$ its lowest order cross section. Initial-state (IS) QED radiative corrections can be described according to the following picture. Before arriving at the annihilation point, the incoming electron (positron) of four-momentum $p_{-(+)}$ radiates real and virtual photons. These photons, due to the dynamical features of QED, are mainly radiated along the direction of motion of the radiating particles, and their effect is mainly to reduce the original four-momentum of the incoming electron (positron) to $x_{1(2)}p_{-(+)}$. After this pre-emission, the hard scattering process $e^-(x_1p_-)e^+(x_2p_+) \rightarrow X$ takes place, at a reduced squared c.m. energy $\hat{s} = x_1x_2s$. The resulting cross section, corrected for IS QED radiation, can be represented as follows [179, 180, 181]

$$\sigma(s) = \int_0^1 dx_1 dx_2 D(x_1, s) D(x_2, s) \sigma_0(x_1 x_2 s) \Theta(\text{cuts}), \quad (27)$$

where $D(x, s)$ is the electron SF, representing the probability that an incoming electron (positron) radiates a collinear photon, retaining a fraction x of its original momentum at the energy scale $Q^2 = s$, and $\Theta(\text{cuts})$ stands for a rejection algorithm taking care of experimental cuts. When considering photonic radiation only the non-singlet part of the SF is of interest. If the running of the QED coupling constant is neglected, the non-singlet part of the SF is the solution of the following Renormalization Group (RG) equation, analogous to the Dokshitzer-Gribov-Lipatov-Altarelli-Parisi (DGLAP) equation of QCD [189, 190, 191]:

$$s \frac{\partial}{\partial s} D(x, s) = \frac{\alpha}{2\pi} \int_x^1 \frac{dz}{z} P_+(z) D\left(\frac{x}{z}, s\right), \quad (28)$$

where $P_+(z)$ is the regularized Altarelli-Parisi (AP) splitting function electron \rightarrow electron + photon, given by

$$P_+(z) = P(z) - \delta(1-z) \int_0^1 dx P(x), \quad (29)$$

$$P(z) = \frac{1+z^2}{1-z}.$$

Equation (28) can be also transformed into an integral equation, subject to the boundary condition $D(x, m_e^2) =$

$\delta(1-x)$:

$$D(x, s) = \delta(1-x) + \frac{\alpha}{2\pi} \int_{m_e^2}^s \frac{dQ^2}{Q^2} \int_x^1 \frac{dz}{z} P_+(z) D\left(\frac{x}{z}, Q^2\right). \quad (30)$$

Eq. (30) can be solved exactly by means of numerical methods, such as the inverse Mellin transform method. However, this derivation of $D(x, s)$ turns out to be problematic in view of phenomenological applications. Therefore, approximate (but very accurate) analytical representations of the solution of the evolution equation are of major interest for practical purposes. This type of solution was the one typically adopted in the context of LEP/SLC phenomenology. A first analytical solution can be obtained in the soft photon approximation, i.e. in the limit $x \simeq 1$. This solution, also known as Gribov-Lipatov (GL) approximation, exponentiates at all perturbative orders the large logarithmic contributions of infrared and collinear origin, but it does not take into account hard-photon (collinear) effects. This drawback can be overcome by solving the evolution equation iteratively. At the n -th step of the iteration, one obtains the $\mathcal{O}(\alpha^n)$ contribution to the SF for any value of x . By combining the GL solution with the iterative one, in which the soft-photon part has been eliminated in order to avoid double counting, one can build a hybrid solution of the evolution equation. It exploits all the positive features of the two kinds of solutions and is not affected by the limitations intrinsic to each of them. Two classes of hybrid solutions, namely the additive and factorized ones, are known in the literature and both were adopted for applications to LEP/SLC precision physics. A typical additive solution, where the GL approximation is supplemented by finite order terms present in the iterative solution, is given by [192]

$$\begin{aligned} D_A(x, s) &= \sum_{i=0}^3 d_A^{(i)}(x, s), \\ d_A^{(0)}(x, s) &= D_{GL}(x, s) = \frac{\exp\left[\frac{1}{2}\beta\left(\frac{3}{4} - \gamma_E\right)\right]}{\Gamma\left(1 + \frac{1}{2}\beta\right)} \frac{1}{2} \beta (1-x)^{\frac{1}{2}\beta-1}, \\ d_A^{(1)}(x, s) &= -\frac{1}{4}\beta(1+x), \\ d_A^{(2)}(x, s) &= \frac{1}{32}\beta^2 \left[(1+x)(-4\ln(1-x) + 3\ln x) \right. \\ &\quad \left. - 4\frac{\ln x}{1-x} - 5 - x \right], \\ d_A^{(3)}(x, s) &= \frac{1}{384}\beta^3 \left\{ (1+x)[18\zeta(2) - 6\text{Li}_2(x) \right. \\ &\quad \left. - 12\ln^2(1-x)] + \frac{1}{1-x} \left[-\frac{3}{2}(1+8x+3x^2)\ln x \right. \right. \\ &\quad \left. \left. + \frac{1}{2}(1+7x^2)\ln^2 x - 12(1+x^2)\ln x \ln(1-x) \right. \right. \\ &\quad \left. \left. - 6(x+5)(1-x)\ln(1-x) \right. \right. \\ &\quad \left. \left. - \frac{1}{4}(39-24x-15x^2) \right] \right\}, \end{aligned} \quad (31)$$

where Γ is the Euler gamma-function, $\gamma_E = \dots$ the Euler-Mascheroni constant, ζ the Riemann ζ -function and β is

the large collinear factor

$$\beta = \frac{2\alpha}{\pi} \left[\ln\left(\frac{s}{m_e^2}\right) - 1 \right]. \quad (32)$$

Explicit examples of factorized solutions, which are obtained by multiplying the GL solution by finite order terms, in such a way that, order by order, the iterative contributions are exactly recovered, can be found in [193]. For the calculation of HO corrections with a per mille accuracy analytical SFs in additive and factorized form containing up to $\mathcal{O}(\alpha^3)$ finite order terms are sufficient and in excellent agreement. They also agree well below the 0.1% level with the exact numerical solution of the QED evolution equation. Explicit solutions up to the fifth order in α were calculated in [194, 195].

The RG method described above was applied in [196] for the treatment of LL QED radiative corrections to various processes of interest for the physics at meson factories. Such a formulation was later implemented in the generator MCGPJ. For example, according to [196], the Bhabha scattering cross section, accounting for LL terms in all orders, $\mathcal{O}(\alpha^n L^n)$, $n = 1, 2, \dots$, of perturbation theory, is given by

$$\begin{aligned} d\sigma_{\text{LLA}}^{\text{Bhabha}} &= \sum_{a,b,c,d=e^{\pm}, \gamma} \int_{\bar{z}_1}^1 dz_1 \int_{\bar{z}_2}^1 dz_2 D_{ae^-}^{\text{str}}(z_1) D_{be^+}^{\text{str}}(z_2) \\ &\quad \times d\sigma_0^{ab \rightarrow cd}(z_1, z_2) \int_{\bar{y}_1}^1 \frac{dy_1}{Y_1} D_{e^-c}^{\text{frg}}\left(\frac{y_1}{Y_1}\right) \int_{\bar{y}_2}^1 \frac{dy_2}{Y_2} D_{e^+d}^{\text{frg}}\left(\frac{y_2}{Y_2}\right) \\ &\quad + \mathcal{O}\left(\alpha^2 L, \alpha \frac{m_e^2}{s}\right), \end{aligned} \quad (33)$$

where $d\sigma_0^{ab \rightarrow cd}(z_1, z_2)$ is the differential LO cross section of the process $ab \rightarrow cd$ with energy fractions of the incoming particles being scaled by factors z_1 and z_2 with respect to the initial electron and positron, respectively. In the notation of [196], the electron SF $D_{ab}^{\text{str}}(z)$ is distinguished from the electron fragmentation function $D_{ab}^{\text{frg}}(z)$ to point out the role played by IS radiation (described by $D_{ab}^{\text{str}}(z)$) with respect to the one due to final-state radiation (described by $D_{ab}^{\text{frg}}(z)$). However, because of their probabilistic meaning, the electron structure and fragmentation functions coincide. In Eq. (33) the quantities $Y_{1,2}$ are the energy fractions of particles c and d with respect to the beam energy. Explicit expressions for $Y_{1,2} = Y_{1,2}(z_1, z_2, \cos\theta)$ and other details on the kinematics can be found in [196]. The lower limits of the integrals, $\bar{z}_{1,2}$ and $\bar{y}_{1,2}$, should be defined according to the experimental conditions of particle registration and kinematical constraints. For the case of $e^+e^- \rightarrow \gamma\gamma$ process, one has to change the master formula (33) by picking up the two photon final state. Formally it can be done just by choosing the proper fragmentation functions, $D_{\gamma c}^{\text{frg}}$ and $D_{\gamma d}^{\text{frg}}$.

The photonic part of the non-singlet electron structure (fragmentation) function in $\mathcal{O}(\alpha^n L^n)$ considered in [196] reads as follows

$$D_{ee}^{NS, \gamma}(z) = \delta(1-z) + \sum_{i=1}^n \left(\frac{\alpha}{2\pi} (L-1) \right)^i \frac{1}{i!} \left[P_{ee}^{(0)}(z) \right]^{\otimes i},$$

$$\begin{aligned}
D_{\gamma e}(z) &= \frac{\alpha}{2\pi}(L-1)P_{\gamma e}(z) + \mathcal{O}(\alpha^2 L^2), \\
D_{e\gamma}(z) &= \frac{\alpha}{2\pi}LP_{\gamma e}(z) + \mathcal{O}(\alpha^2 L^2), \\
P_{ee}^{(0)}(z) &= \left[\frac{1+z^2}{1-z} \right]_+ \\
&= \lim_{\Delta \rightarrow 0} \left\{ \delta(1-z)(2\ln \Delta + \frac{3}{2}) + \Theta(1-z-\Delta) \frac{1+z^2}{1-z} \right\}, \\
[P_{ee}^{(0)}(z)]^{\otimes i} &= \int_z^1 \frac{dt}{t} P_{ee}^{(i-1)}(t) P_{ee}^{(0)}\left(\frac{z}{t}\right), \\
P_{e\gamma}(z) &= z^2 + (1-z)^2, \quad P_{\gamma e}(z) = \frac{1+(1-z)^2}{z}.
\end{aligned} \tag{34}$$

Starting from the second order in α there appear also non-singlet and singlet e^+e^- pair contributions to the structure function:

$$\begin{aligned}
D_{ee}^{NS,e^+e^-}(z) &= \frac{1}{3} \left(\frac{\alpha}{2\pi} L \right)^2 P_{ee}^{(1)}(z) + \mathcal{O}(\alpha^3 L^3), \\
D_{ee}^{S,e^+e^-}(z) &= \frac{1}{2!} \left(\frac{\alpha}{2\pi} L \right)^2 R(z) + \mathcal{O}(\alpha^3 L^3), \\
R(z) &= P_{e\gamma} \otimes P_{\gamma e}(z) = \frac{1-z}{3z} (4+7z+4z^2) + 2(1+z) \ln z.
\end{aligned}$$

Note that radiation of a real pair, *i.e.* appearance of additional electrons and positrons in the final state, require application of nontrivial conditions of experimental particle registration. Unambiguously, that can be done only within a Monte Carlo event generator based on four-particle matrix elements, as already discussed in the Section 1.4.

In the same way as in QCD, the LLA cross sections depend on the choice of the factorization scale Q^2 in the argument of the large logarithm $L = \ln(Q^2/m_e^2)$, which is not fixed a priori by the theory. However, the scale should be taken of the order of the characteristic energy transfer in the process under consideration. Typical choices are $Q^2 = s$, $Q^2 = -t$, and $Q^2 = st/u$. The first one is good for annihilation channels, like $e^+e^- \rightarrow \mu^+\mu^-$, the second one is optimal for small-angle Bhabha scattering, where the t -channel exchange dominates, see [197]. The last choice allows to exponentiate the leading contribution due to initial-final state interference [198] and is particularly suited for large-angle Bhabha scattering in QED. The option $Q^2 = st/u$ is adopted in all the versions of the generator BabaYaga. Reduction of the scale dependence can be achieved by taking into account next-to-leading corrections in $\mathcal{O}(\alpha^n L^{n-1})$, next-to-next-to-leading ones in $\mathcal{O}(\alpha^n L^{n-2})$ *etc.*

The Parton Shower algorithm

The PS algorithm is a method for providing a Monte Carlo iterative solution of the evolution equation, at the same time generating the four-momenta of the electron and photon at a given step of the iteration. It was developed within the context of QCD and later applied in QED too.

In order to implement the algorithm, it is first necessary to assume the existence of an upper limit for the

energy fraction x , in such a way that the AP splitting function is regularized as follows:

$$P_+(z) = \theta(x_+ - z)P(z) - \delta(1-z) \int_0^{x_+} dx P(x). \tag{35}$$

Of course, in the limit $x_+ \rightarrow 1$ Eq. (35) recovers the usual definition of the AP splitting function given in Eq. (29). By inserting the modified AP vertex into Eq. (28), one obtains

$$\begin{aligned}
s \frac{\partial}{\partial s} D(x, s) &= \frac{\alpha}{2\pi} \int_x^{x_+} \frac{dz}{z} P(z) D\left(\frac{x}{z}, s\right) \\
&\quad - \frac{\alpha}{2\pi} D(x, s) \int_x^{x_+} dz P(z).
\end{aligned} \tag{36}$$

Separating the variables and introducing the Sudakov form factor

$$\Pi(s_1, s_2) = \exp \left[-\frac{\alpha}{2\pi} \int_{s_2}^{s_1} \frac{ds'}{s'} \int_0^{x_+} dz P(z) \right], \tag{37}$$

which is the probability that the electron evolves from virtuality $-s_2$ to $-s_1$ without emitting photons of energy fraction larger than $1 - x_+ \equiv \epsilon$ ($\epsilon \ll 1$), Eq. (36) can be recast into integral form as follows:

$$\begin{aligned}
D(x, s) &= \Pi(s, m_e^2) D(x, m_e^2) \\
&\quad + \frac{\alpha}{2\pi} \int_{m_e^2}^s \frac{ds'}{s'} \Pi(s, s') \int_x^{x_+} \frac{dz}{z} P(z) D\left(\frac{x}{z}, s'\right)
\end{aligned} \tag{38}$$

The formal iterative solution of Eq. (38) can be represented by the following infinite series:

$$\begin{aligned}
D(x, s) &= \sum_{n=0}^{\infty} \prod_{i=1}^n \left\{ \int_{m_e^2}^{s_{i-1}} \frac{ds_i}{s_i} \Pi(s_{i-1}, s_i) \right. \\
&\quad \times \left. \frac{\alpha}{2\pi} \int_{x/(z_1 \cdots z_{i-1})}^{x_+} \frac{dz_i}{z_i} P(z_i) \right\} \Pi(s_n, m_e^2) D\left(\frac{x}{z_1 \cdots z_n}, m_e^2\right).
\end{aligned} \tag{39}$$

The particular form of Eq. (39) allows to exploits a Monte Carlo method for building the solution iteratively. The steps of the algorithm are as follows:

- 1 – set $Q^2 = m_e^2$, and fix $x = 1$ according to the boundary condition $D(x, m_e^2) = \delta(1-x)$;
- 2 – generate a random number ξ in the interval $[0, 1]$;
- 3 – if $\xi < \Pi(s, Q^2)$ stop the evolution; otherwise
- 4 – compute Q'^2 as a solution of the equation $\xi = \Pi(Q'^2, Q^2)$;
- 5 – generate a random number z according to the probability density $P(z)$ in the interval $[0, x_+]$;
- 6 – substitute $x \rightarrow xz$ and $Q^2 \rightarrow Q'^2$; go to 2.

The x distribution of the electron SF as obtained through the PS algorithm and a numerical solution (based on the inverse Mellin transform method) of the QED DGLAP equation is shown in Fig. 14. Perfect agreement is seen. Once $D(x, s)$ has been reconstructed by the algorithm, the master formula of Eq. (27) can be used for the calculation

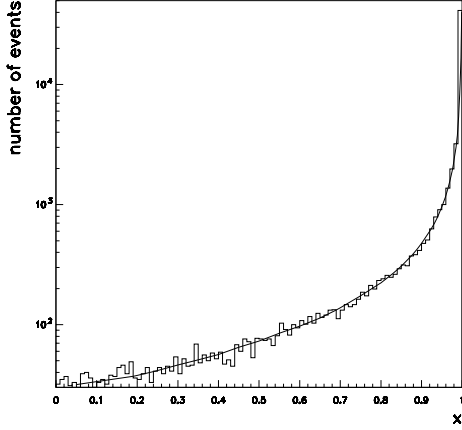


Fig. 14. Comparison for the x distribution of the electron SF at $\sqrt{s} = 190$ GeV, as obtained by means of a numerical solution of the QED evolution equation (solid line) and the PS algorithm (histogram).

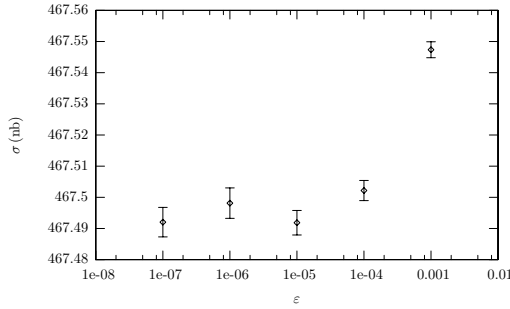


Fig. 15. QED corrected Bhabha cross section at DAΦNE as a function of the infrared regulator ϵ of the PS approach, according to set up of Eq. (??). The error bars correspond to 1σ Monte Carlo error.

of LL corrections to the cross section of interest. This cross section must be independent on the soft-hard photon separator ϵ , in the limit of small ϵ values. This can be clearly seen in Fig. 15, where the QED corrected Bhabha cross section as a function of the fictitious parameter ϵ is shown at DAΦNE energies, according to the cuts of Eq. (12), for an angular acceptance θ_{\pm} of $55^{\circ} \div 125^{\circ}$. The cross section reaches a plateau for ϵ smaller than 10^{-4} .

The main advantage of the PS algorithm with respect to the analytical solutions of the electron evolution is the possibility of going beyond the strictly collinear approximation and generating transverse momentum p_{\perp} of electrons and photons at each branching. In fact, the kinematics of the branching process $e(p) \rightarrow e'(p') + \gamma(q)$ can be written as

$$p = (E, \mathbf{0}, p_z), \quad p' = (zE, \mathbf{p}_{\perp}, p'_z), \quad q = ((1-z)E, -\mathbf{p}_{\perp}, q_z) \quad (40)$$

Once the variables p^2 , p'^2 and z are generated by the PS algorithm, the on-shell condition $q^2 = 0$, together with the longitudinal momentum conservation, allows to obtain an

expression for the p_{\perp} variable:

$$p_{\perp}^2 = (1-z)(zp^2 - p'^2) \quad (41)$$

at first order in $p^2/E^2 \ll 1$, $p'^2/E^2 \ll 1$.

However, some not correct behaviours of the exclusive photon kinematics reconstruction are connected with this PS picture, due to the approximations inherent Eq. (41). First of all, since within the PS algorithm the generation of p'^2 and z are independent, it can happen that in some branching the p_{\perp}^2 as given by Eq. (41) is negative. In order to avoid this problem, the introduction of any kinematical cut on p^2 or z generation (or the regeneration of the whole event) would mean a not correct reconstruction of the SF x distribution, which is important for a precise cross section calculation. Furthermore, in the PS scheme, each fermion produces its photons cascade independently from the other ones, missing the effects due to the interference of radiation coming from different charged particles. As far as inclusive cross sections (i.e., no cuts are imposed on the generated photons) are considered, these effects are largely integrated out but they become important when more exclusive variables distributions are looked at, as shown in [199]

Concerning the first problem, it can be overcome choosing a generation of photons p_{\perp} different from Eq. (41). For example, one can choose to extract the photon $\cos\vartheta_{\gamma}$ according to the universal leading poles $1/p \cdot k$ present in the matrix element for photon emission. Namely, one can generate $\cos\vartheta_{\gamma}$ as

$$\cos\vartheta_{\gamma} \propto \frac{1}{1 - \beta \cos\vartheta_{\gamma}}, \quad (42)$$

where β is the speed of the emitting particle. In this way, photon energy and angle are generated independently, differently from Eq. (41). The nice feature of this prescription is that $p_{\perp}^2 = E_{\gamma}^2 \sin^2\vartheta_{\gamma}$ is always well defined and the x distribution reproduces exactly the SF, because any further kinematical cuts must be imposed to avoid unphysical events. At this stage, the PS is used only to generate photons energies and photons multiplicity. The problem of including the radiation interference is still unsolved, because the variables of photons emitted by a fermion are still uncorrelated with those of the other charged particles. The issue of including photon interference can be successfully worked out looking at the YFS formula [183]:

$$d\sigma_n \approx d\sigma_0 \frac{e^{2n}}{n!} \prod_{l=1}^n \frac{d^3\mathbf{k}_l}{(2\pi)^3 2k_l^0} \sum_{i,j=1}^N \eta_i \eta_j \frac{-p_i \cdot p_j}{(p_i \cdot k_l)(p_j \cdot k_l)}. \quad (43)$$

It gives the differential cross section $d\sigma_n$ for the emission of n photons, whose momenta are k_1, \dots, k_n , from a kernel process described by $d\sigma_0$ and involving N fermions, whose momenta are p_1, \dots, p_N . In Eq. (43), η_i is a charge factor, which is $+1$ for incoming e^- or outgoing e^+ and -1 for incoming e^+ or outgoing e^- . Note that Eq. (43) is valid in the soft limit ($k_i \rightarrow 0$). The important point is that it also accounts for coherence effects. From YFS formula, it

is straightforward to read out the angular spectrum of the l^{th} photon:

$$\cos \vartheta_l \propto - \sum_{i,j=1}^N \eta_i \eta_j \frac{1 - \beta_i \beta_j \cos \vartheta_{ij}}{(1 - \beta_i \cos \vartheta_{il})(1 - \beta_j \cos \vartheta_{jl})} . \quad (44)$$

It is worth noticing that in the LL prescription, the same quantity writes as

$$\cos \vartheta_l \propto \sum_{i=1}^N \frac{1}{1 - \beta_i \cos \vartheta_{il}} \quad (45)$$

whose terms are of course contained in Eq. (44).

In order to consider also coherence effects in the angular distribution of the photons, one can generate $\cos \vartheta_\gamma$ according to Eq. (44), rather than Eq. (45). This recipe [199] is adopted in BabaYaga v3.5 and BabaYaga@NLO.

Yennie-Frautschi-Suura exponentiation

The YFS exponentiation procedure, implemented in the code BHWIDE, is a technique for summing up all the infra-red (IR) singularities present in any process accompanied by photonic radiation [183]. It is inherently exclusive, i.e. all the summations of the IR-singular contributions are done before any phase-space integration over the virtual- or real-photon four-momenta are performed. The method was mainly developed by S. Jadach, B.F.L. Ward and collaborators to realize precision MC tools. In the following, the general idea underlying the procedure are summarized.

Let us consider, for definiteness, the scattering process $e^+(p_1)e^-(p_2) \rightarrow f_1(q_1) \cdots f_n(q_n)$, where $f_1(q_1) \cdots f_n(q_n)$ represents a given arbitrary final state, and let \mathcal{M}_0 be its tree-level matrix element. By using standard Feynman-diagram techniques, it is possible to show that the same process, when accompanied by l additional real photons radiated by the IS particles, and under the assumption that the l additional photons are soft, i.e. their energy is much smaller than any energy scale involved in the process, can be described by the factorized matrix element built up by the lowest order one, \mathcal{M}_0 , times the product of l eikonal currents, namely

$$\mathcal{M} \simeq \mathcal{M}_0 \prod_{i=1}^l \left[e \left(\frac{\varepsilon_i(k_i) \cdot p_2}{k_i \cdot p_2} - \frac{\varepsilon_i(k_i) \cdot p_1}{k_i \cdot p_1} \right) \right], \quad (46)$$

where e is the electron charge, k_i are the momenta of the photons and $\varepsilon_i(k_i)$ their polarization vectors. Taking the square of the matrix element in Eq. (46) and multiplying for the proper flux factor and the Lorentz-invariant the cross section for the process $e^+(p_1)e^-(p_2) \rightarrow f_1(q_1) \cdots f_n(q_n) + l \text{ real photons}$ can be written as

$$d\sigma_r^{(l)} = d\sigma_0 \frac{1}{l!} \prod_{i=1}^l \left[k_i dk_i d\cos \vartheta_i d\varphi_i \frac{1}{2(2\pi)^3} \sum_{\varepsilon_i} e^2 \left(\frac{\varepsilon_i(k_i) \cdot p_2}{k_i \cdot p_2} - \frac{\varepsilon_i(k_i) \cdot p_1}{k_i \cdot p_1} \right)^2 \right]. \quad (47)$$

By summing on the number of final-state photons, one obtains the cross section for the original process accompanied by an arbitrary number of real photons, namely

$$\begin{aligned} d\sigma_r^{(\infty)} &= \sum_{l=0}^{\infty} d\sigma_r^{(l)} \\ &= d\sigma_0 \exp \left[k dk d\cos \vartheta d\varphi \frac{1}{2(2\pi)^3} \sum_{\varepsilon} e^2 \left(\frac{\varepsilon(k) \cdot p_2}{k \cdot p_2} - \frac{\varepsilon(k) \cdot p_1}{k \cdot p_1} \right)^2 \right]. \end{aligned} \quad (48)$$

Equation (48), being limited to real radiation only, is IR divergent once the phase space integrations are performed down to zero photonic energy. This problem, as well known, finds its solution in the matching between real and virtual photonic radiation. At any rate, Eq. (48) already shows the key feature of exclusive exponentiation, i.e. summing up all the perturbative contributions before performing any phase space integration.

In order to get meaningful radiative corrections, besides IS real photon corrections it is necessary to consider also IS virtual photon corrections, i.e. the corrections due to additional internal photon lines connecting the IS electron and positron. For a vertex-type amplitude, the result can be written as

$$\begin{aligned} \mathcal{M}_{V_1} &= -i \frac{e^2}{(2\pi)^4} \int d^4k \frac{1}{k^2 + i\varepsilon} \bar{v}(p_1) \gamma^\mu \frac{-(\not{p}_1 + \not{k}) + m}{2p_1 \cdot k + k^2 + i\varepsilon} \\ &\quad \times \Gamma \frac{(\not{p}_2 + \not{k}) + m}{2p_2 \cdot k + k^2 + i\varepsilon} \gamma_\mu u(p_2), \end{aligned} \quad (49)$$

where Γ stands for the Dirac structure competing to the lowest order process, in such a way that $\mathcal{M}_0 = \bar{v}(p_1) \Gamma u(p_2)$. The soft-photon part of the amplitude can be extracted by taking $k^\mu \simeq 0$ in all the numerators. In this approximation, the amplitude of Eq. (49) becomes

$$\begin{aligned} \mathcal{M}_{V_1} &= \mathcal{M}_0 \times V \\ V &= \frac{2i\alpha}{(2\pi)^3} \int d^4k \frac{1}{k^2 + i\varepsilon} \frac{4p_1 \cdot p_2}{(2p_1 \cdot k + k^2 + i\varepsilon)(2p_2 \cdot k + k^2 + i\varepsilon)}. \end{aligned} \quad (50)$$

It can be seen that, as in the real case, the IR virtual correction factorizes off the LO matrix element, so that it is universal, i.e. independent of the details of the process under consideration, and is divergent in the IR portion of the phase space.

The correction given by n soft virtual photons can be seen to factorize with an additional $1/n!$ factor, namely

$$\mathcal{M}_{V_n} = \mathcal{M}_0 \times \frac{1}{n!} V^n, \quad (51)$$

so that by summing over all the additional soft virtual photons one obtains

$$\mathcal{M}_V = \mathcal{M}_0 \times \exp[V]. \quad (52)$$

As already noticed, both the real and virtual factors are IR divergent. In order to obtain meaningful expressions, one has to adopt some regularization procedure. One possible regularization procedure is to give the photon a (small) mass λ and modifying eqs. (47) and (50) accordingly. Once all the expressions are properly regularized, one can write down the YFS master formula, which takes into account real and virtual photonic corrections to the LO process. In virtue of the factorization properties discussed above, the master formula can be obtained from Eq. (48) with the substitution $d\sigma_0 \rightarrow d\sigma_0 |\exp(V)|^2$, i.e.

$$d\sigma = d\sigma_0 |\exp(V)|^2 \exp \left[k dk d \cos \vartheta d\varphi \frac{1}{2(2\pi)^3} \sum_{\epsilon} e^2 \left(\frac{\epsilon(k) \cdot p_2}{k \cdot p_2} - \frac{\epsilon(k) \cdot p_1}{k \cdot p_1} \right)^2 \right]. \quad (53)$$

As a last step, it is possible to perform analytically the IR cancellation between virtual and very soft real photons. Actually, since very soft real photons do not affect the kinematics of the process, the real photon exponent can be split into a contribution coming from photons with energy less than a cutoff k_{min} plus a contribution coming from photons with energy above the same cutoff. The first contribution can be integrated over all its phase space and then combined with the virtual exponent. After this step it is possible to remove the regularizing photon mass by taking the limit $\lambda \rightarrow 0$, so that Eq. (53) becomes

$$d\sigma = d\sigma_0 \exp(Y) \exp \left[k dk d\Theta(k - k_{min}) \cos \vartheta d\varphi \frac{1}{2(2\pi)^3} \sum_{\epsilon} e^2 \left(\frac{\epsilon(k) \cdot p_2}{k \cdot p_2} - \frac{\epsilon(k) \cdot p_1}{k \cdot p_1} \right)^2 \right], \quad (54)$$

where Y is given by

$$Y = 2V + \int k dk d\Theta(k_{min} - k) \cos \vartheta d\varphi \frac{1}{2(2\pi)^3} \sum_{\epsilon} e^2 \left(\frac{\epsilon(k) \cdot p_2}{k \cdot p_2} - \frac{\epsilon(k) \cdot p_1}{k \cdot p_1} \right)^2. \quad (55)$$

The explicit form of Y can be derived by performing all the details of the calculation, and reads

$$Y = \beta \ln \frac{k_{min}}{E} + \delta_{YFS}, \quad \delta_{YFS} = \frac{1}{4}\beta + \frac{\alpha}{\pi} \left(\frac{\pi^2}{3} - \frac{1}{2} \right), \quad (56)$$

1.5.2 Matching NLO and higher-order corrections

As it will be shown numerically in Section 1.7, NLO corrections must be combined with multiple photon emission effects to achieve a theoretical accuracy at the per mille level. This combination, technically known as *matching*, is on the grounds of the most precise generators used for luminosity monitoring, i.e. BabaYaga@NLO, BHWIDE, and

MCGPJ. Although the matching is implemented according to different theoretical details, some general aspects are common to all the recipes and must be emphasized:

1. it is possible to match NLO and HO corrections consistently, avoiding double counting of LL contributions at order α and preserving the advantages of resummation of soft and collinear effects beyond $O(\alpha)$;
2. the convolution of NLO corrections with HO terms allows to include, *even if approximately*, the dominant part of NNLO corrections, given by infrared-enhanced $\alpha^2 L$ sub-leading contributions. This was argued and demonstrated analytically and numerically in [200] through comparison with the available $O(\alpha^2)$ corrections to s -channel processes and t -channel Bhabha scattering. Such an aspect of the matching procedure is crucial to settle the theoretical accuracy of the generators by means of explicit comparisons with the exact NNLO perturbative corrections discussed in Section 1.4, and will be addressed in Section 1.9
3. BabaYaga@NLO and BHWIDE implement a fully factorized matching recipe, while MCGPJ include some terms in additive form, as visible in the formulae reported in the following. This can give rise to some (minor) differences, when performing tuned comparisons between the programs predictions.

Remarkably, the topic of matching is one of the most important advances in modern perturbative QCD and electroweak calculations for physics at hadron colliders. The NLO QCD corrections were matched with QCD PS in [201, 202, 203, 204] and such approaches gave rise to the codes MC@NLO and POWHEG used for simulations of many processes in hadronic collisions. For the Drell-Yan-like processes, the complete $O(\alpha)$ electroweak corrections were combined with QED/QCD shower evolution and implemented in the generator HORACE [205, 206]. It is currently used for the precision measurement of the W -boson mass at the Fermilab Tevatron and for preliminary investigations in view of the early data at the CERN LHC.

In the following we summarize the basic features of the matching procedure as implemented in the codes MCGPJ and BabaYaga@NLO. For BHWIDE, the interested reader is referred to the original literature [188].

The matching approach realized in the MC event generator MCGPJ was developed in [187]. In particular, Bhabha scattering with complete $O(\alpha)$ and HO LL photonic corrections is represented in the following way:

$$\begin{aligned} \frac{d\sigma^{e^+e^- \rightarrow e^+e^-(\gamma)}}{d\Omega_-} &= \int_{\bar{z}_1}^1 dz_1 \int_{\bar{z}_2}^1 dz_2 D_{ee}^{NS,\gamma}(z_1) D_{ee}^{NS,\gamma}(z_2) \\ &\times \frac{d\hat{\sigma}_0^{\text{Bhabha}}(z_1, z_2)}{d\Omega_-} \left(1 + \frac{\alpha}{\pi} K_{SV} \right) \Theta(\text{cuts}) \\ &\times \int_{y_{th}}^{Y_1} \frac{dy_1}{Y_1} \int_{y_{th}}^{Y_2} \frac{dy_2}{Y_2} D_{ee}^{NS,\gamma}\left(\frac{y_1}{Y_1}\right) D_{ee}^{NS,\gamma}\left(\frac{y_2}{Y_2}\right) \end{aligned}$$

$$\begin{aligned}
& + \frac{\alpha}{\pi} \int_{\Delta} \frac{dx}{x} \left\{ \left[\left(1 - x + \frac{x^2}{2} \right) \ln \frac{\theta_0^2 (1-x)^2}{4} + \frac{x^2}{2} \right] \right. \\
& \times 2 \frac{d\sigma_0^{\text{Bhabha}}}{d\Omega_-} + \left[\left(1 - x + \frac{x^2}{2} \right) \ln \frac{\theta_0^2}{4} + \frac{x^2}{2} \right] \\
& \times \left[\frac{d\hat{\sigma}_0^{\text{Bhabha}}(1-x, 1)}{d\Omega_-} + \frac{d\hat{\sigma}_0^{\text{Bhabha}}(1, 1-x)}{d\Omega_-} \right] \left. \right\} \Theta(\text{cuts}) \\
& - \frac{\alpha^2}{4s} \left(\frac{3+c^2}{1-c} \right)^2 \frac{8\alpha}{\pi} \ln(\text{ctg} \frac{\theta}{2}) \ln \frac{\Delta\varepsilon}{\varepsilon} \\
& + \frac{\alpha^3}{2\pi^2 s} \int_{\substack{k^0 > \Delta\varepsilon \\ \theta_i > \theta_0}} \frac{WT}{4} \Theta(\text{cuts}) \frac{d\Gamma_{e\bar{e}\gamma}}{d\Omega_-}. \quad (57)
\end{aligned}$$

Here the step functions $\Theta(\text{cuts})$ stand for the particular applied cuts. The auxiliary parameter θ_0 defines cones around the directions of charged particles motion in which the emission of hard photons is approximated by the factorized form by convolution of collinear radiation factors [207] with the Born cross section. The dependence on the parameters Δ and θ_0 cancels out in the sum with the last term of Eq. (57), where the photon energy and emission angles with respect to all charged particles are limited from below ($k^0 > \Delta\varepsilon, \theta_i > \theta_0$). Taking into account vacuum polarization, the Born level Bhabha cross section with reduced energies of the incoming electron and positron can be cast in the following form:

$$\begin{aligned}
\frac{d\hat{\sigma}_0^{\text{Bhabha}}(z_1, z_2)}{d\Omega_-} &= \frac{4\alpha^2}{s a^2} \left\{ \frac{1}{|1 - \Pi(\hat{t})|^2} \frac{a^2 + z_2^2(1+c)^2}{2z_1^2(1-c)^2} \right. \\
&+ \frac{1}{|1 - \Pi(\hat{s})|^2} \frac{z_1^2(1-c)^2 + z_2^2(1+c)^2}{2a^2} \\
&- \text{Re} \frac{1}{(1 - \Pi(\hat{t}))(1 - \Pi(\hat{s}))^*} \frac{z_2^2(1+c)^2}{a z_1(1-c)} \left. \right\} d\Omega_-, \\
\hat{s} &= z_1 z_2 s, \quad \hat{t} = -\frac{s z_1^2 z_2 (1-c)}{z_1 + z_2 - (z_1 - z_2)c}. \quad (58)
\end{aligned}$$

where $\Pi(Q^2)$ is the photon self-energy correction. Note that in the cross section above the cosine of the scattering angle, c , is given for the original c.m. reference frame of the colliding beams.

For the two photon production channel, a similar representation is used in MCGPJ:

$$\begin{aligned}
d\sigma^{e^+e^- \rightarrow \gamma\gamma(\gamma)} &= \int_{\hat{z}_1}^1 dz_1 D_{ee}^{NS, \gamma}(z_1) \int_{\hat{z}_2}^1 dz_2 D_{ee}^{NS, \gamma}(z_2) \\
&\times d\hat{\sigma}_0^{\gamma\gamma}(z_1, z_2) \left(1 + \frac{\alpha}{\pi} K_{SV}^{\gamma\gamma} \right) + \frac{\alpha}{\pi} \int_{\Delta} \frac{dx}{x} \\
&\times \left[\left(1 - x + \frac{x^2}{2} \right) \ln \frac{\theta_0^2}{4} + \frac{x^2}{2} \right] \left[d\hat{\sigma}_0(1-x, 1) \right. \\
&+ d\hat{\sigma}_0(1, 1-x) \left. \right] + \frac{1}{3} \frac{4\alpha^3}{\pi^2 s^2} \int_{\substack{z_i \geq \Delta \\ \pi - \theta_0 \geq \theta_i \geq \theta_0}} d\Gamma_{3\gamma}
\end{aligned}$$

$$\begin{aligned}
&\times \left[\frac{z_3^2(1+c_3^2)}{z_1^2 z_2^2 (1-c_1^2)(1-c_2^2)} + \text{two cyclic permutations} \right], \\
z_i &= \frac{q_i^0}{\varepsilon}, \quad c_i = \cos \theta_i, \quad \theta_i = \widehat{\mathbf{p} - \mathbf{q}_i}, \quad (59)
\end{aligned}$$

where the cross section with reduced energies has the form

$$\frac{d\hat{\sigma}_0^{\gamma\gamma}(z_1, z_2)}{d\Omega_1} = \frac{2\alpha^2}{s} \frac{z_1^2(1-c_1)^2 + z_2^2(1+c_1)^2}{(1-c_1^2)(z_1+z_2+(z_2-z_1)c_1)^2},$$

and the factor 1/3 in the last term of Eq. (59) takes into account the identity of the final photons. The sum of the last two terms does not depend on Δ and θ_0 .

Concerning BabaYaga@NLO, the matching starts from the observation that Eq. (27) for the QED corrected all-order cross section can be rewritten, in terms of the PS ingredients, as

$$d\sigma_{LL}^{\infty} = \Pi(Q^2, \varepsilon) \sum_{n=0}^{\infty} \frac{1}{n!} |\mathcal{M}_{n,LL}|^2 d\Phi_n \quad (60)$$

The expansion at $\mathcal{O}(\alpha)$ of Eq. (60) does not coincide, by construction, with an exact $\mathcal{O}(\alpha)$ result. In fact

$$\begin{aligned}
d\sigma_{LL}^{\alpha} &= \left[1 - \frac{\alpha}{2\pi} I_+ \log \frac{Q^2}{m^2} \right] |\mathcal{M}_0|^2 d\Phi_0 + |\mathcal{M}_{1,LL}|^2 d\Phi_1 \\
&\equiv [1 + C_{\alpha,LL}] |\mathcal{M}_0|^2 d\Phi_0 + |\mathcal{M}_{1,LL}|^2 d\Phi_1 \quad (61)
\end{aligned}$$

whereas an exact NLO cross section can be always cast in the form

$$d\sigma^{\alpha} = [1 + C_{\alpha}] |\mathcal{M}_0|^2 d\Phi_0 + |\mathcal{M}_1|^2 d\Phi_1 \quad (62)$$

The coefficient C_{α} contains the complete virtual $\mathcal{O}(\alpha)$ and the $\mathcal{O}(\alpha)$ soft-bremsstrahlung squared matrix elements, in units of the Born squared amplitude, and $|\mathcal{M}_1|^2$ is the exact squared matrix element with the emission of one hard photon. We remark that $C_{\alpha,LL}$ has the same logarithmic structure as C_{α} and that $|\mathcal{M}_{1,LL}|^2$ has the same singular behaviour of $|\mathcal{M}_1|^2$.

In order to match the LL and NLO calculations, the following correction factors, which are by construction infrared safe and free of collinear logarithms, are introduced

$$F_{SV} = 1 + (C_{\alpha} - C_{\alpha,LL}), \quad F_H = 1 + \frac{|\mathcal{M}_1|^2 - |\mathcal{M}_{1,LL}|^2}{|\mathcal{M}_{1,LL}|^2} \quad (63)$$

so that the exact $\mathcal{O}(\alpha)$ cross section can be expressed, up to terms of $\mathcal{O}(\alpha^2)$, in terms of its LL approximation as

$$d\sigma^{\alpha} = F_{SV} (1 + C_{\alpha,LL}) |\mathcal{M}_0|^2 d\Phi_0 + F_H |\mathcal{M}_{1,LL}|^2 d\Phi_1 \quad (64)$$

Driven by Eq. (64), Eq. (60) can be improved by writing the resummed cross section as

$$d\sigma_{matched}^{\infty} = F_{SV} \Pi(Q^2, \varepsilon) \sum_{n=0}^{\infty} \frac{1}{n!} \left(\prod_{i=0}^n F_{H,i} \right) |\mathcal{M}_{n,LL}|^2 d\Phi_n \quad (65)$$

The correction factors $F_{H,i}$ follow from the definition Eq. (63) for each photon emission. The expansion at $\mathcal{O}(\alpha)$ of Eq. (65)

Table 2. MC generators used for luminosity monitoring at meson factories.

Generator	Theory	Accuracy
Bagenf	$O(\alpha)$	$\sim 1\%$
BabaYaga v3.5	Parton Shower	$0.5 \div 1\%$
BabaYaga@NLO	$O(\alpha) + \text{PS}$	$\sim 0.1\%$
BHWIDE	$O(\alpha)$ YFS	$\sim 0.5\%$ (LEP1)
BKQED	$O(\alpha)$	$\sim 1\%$
MCGPJ	$O(\alpha) + \text{SF}$	$< 0.2\%$

coincides now with the exact NLO cross section Eq. (62) and all higher order LL contributions are the same as in Eq. (60). This formulation is implemented in BabaYa@NLO for both Bhabha scattering and photon pair production, using, of course, the appropriate SV and hard bremsstrahlung formulae.

As the SF method, the method of YFS exclusive exponentiation can be improved in order to take into account HO corrections on top of finite-order exact results (see for instance [188] and references therein).

1.6 Monte Carlo generators

The software tools used in early measurements of luminosity at flavour factories (and sometimes still used in recent experimental publications) include generators such as Bagenf [208], BabaYaga v3.5 [185] and BKQED [209, 210]. However, the above MC programs either are based on a fixed NLO calculation (such as Bagenf and BKQED) or include corrections to all orders in perturbation theory, but in the LL approximation only (like BabaYaga v 3.5). Therefore, the precision of these codes can be estimated to lie in the range $0.5 \div 1\%$, depending on the adopted experimental cuts.

The increasing precision reached on the experimental side during the last few years led to the development of new, dedicated theoretical tools, such as BabaYaga@NLO and MCGPJ, and the adoption of already well-tested codes, such as BHWIDE, the latter extensively used at high-energy LEP/SLC colliders for simulation of the large-angle Bhabha process. As already emphasized in Section 1.5.2, all these three codes include NLO corrections in combination with multiple photon contributions and have, therefore, a precision tag of $\sim 0.1\%$.

A list of the MC tools used in the luminosity measurement at meson factories is given in Tab. 2, which summarizes the main ingredients of their formulation for radiative corrections and the estimate of their theoretical accuracy.

The basic theoretical and phenomenological features of the different generators are summarized in the following.

1. Bagenf/BKQED – BKQED is the event generator developed by Berends and Kleiss and based on the classical, exact NLO calculations of [209, 210] for all QED processes. It was significantly used at LEP, especially for the simulation of the $e^+e^- \rightarrow \gamma\gamma$ process. Bagenf is

a code realized by Drago and Venanzoni at the beginning of DAΦNE operation to simulate Bhabha events, adapting the calculations of [209] to include the contribution of the Φ resonance. Both generators lack the effect of HO corrections and, as such, have a precision accuracy of about 1%.

2. BabaYaga v3.5 – It is a MC generator developed by the Pavia group at the starting of DAΦNE operation using a QED PS approach for the treatment of LL QED corrections to luminosity processes and later improved to account for the interference of radiation emitted by different charged legs in the generation of the momenta of the final-state particles. The main drawback of BabaYaga v3.5 is the absence of $O(\alpha)$ non-log contributions, resulting in a theoretical precision of $\sim 0.5\%$ for large-angle Bhabha scattering and of about 1% for $\gamma\gamma$ and $\mu^+\mu^-$ final states.
3. BabaYaga@NLO – It is the presently released version of BabaYaga, based on the matching of exact $O(\alpha)$ corrections with QED PS, as described in Section 1.5.2. The accuracy of the current version is estimated to be at 0.1% level for large-angle Bhabha scattering, two-photon and $\mu^+\mu^-$ production. Like BabaYaga v3.5, BabaYaga@NLO is available at the web page of the Pavia phenomenology group www.pv.infn.it/~hepcomplex/babayaga.html.
4. BHWIDE – It is a MC code realized in Krakow-Knoxville at the time of LEP operation and described in [188]. In this generator, exact $O(\alpha)$ corrections are matched with the resummation of soft and collinear logarithms through the YFS exponentiation approach. According to the authors, the precision is estimated about 0.5% for LEP1. This accuracy estimate was derived through detailed comparisons of the BHWIDE predictions with those of other LEP tools in the presence of the full set of NLO corrections, including purely weak corrections. However, since the latter are phenomenologically unimportant at e^+e^- accelerators of moderately high energies and the QED theoretical ingredients of BHWIDE are very similar to the formulation of both BabaYaga@NLO and MCGPJ, one can argue that BHWIDE accuracy for physics at flavour factories is at the level of 0.1%. The code is available at placzek.home.cern.ch/placzek/bhwide/.
5. MCGPJ – It is the generator developed by a Dubna-Novosibirsk collaboration and used at VEPP collider. This program includes exact $O(\alpha)$ corrections supplemented with HO LL contributions related to the emission of collinear photon jets and taken into account through collinear QED Structure Functions (SF). The theoretical precision is estimated to be better than 0.2%.

It is worth noticing that the theoretical uncertainty of the most accurate generators, based on the matching of exact NLO with LL resummation, starts at the level of

⁷ At present, finite mass effects in the virtual corrections to $e^+e^- \rightarrow \mu^+\mu^-$, which should be taken into for precision simulations at the Φ -factories, are not included in BabaYaga@NLO.

Table 3. Bhabha cross section (in nb) at meson factories according to different precision levels and using the cuts of Eq. (12), but with an angular acceptance of $55^\circ \leq \theta_\pm \leq 125^\circ$. The numbers in parenthesis are 1σ MC errors.

$\sqrt{s}(\text{GeV})$	1.02	4	10
σ_0	529.4631(2)	44.9619(1)	5.5026(2)
σ_0^{VP}	542.657(6)	46.9659(1)	5.85526(3)
σ_{NLO}	451.523 (6)	37.1654 (6)	4.4256 (2)
$\sigma_\alpha^{\text{PS}}$	454.503 (6)	37.4186 (6)	4.4565 (1)
σ_{matched}	455.858 (5)	37.6731 (4)	4.5046 (3)
σ^{PS}	458.437 (4)	37.8862 (4)	4.5301 (2)

sub-leading NNLO contributions, as far as photonic corrections are concerned. Other sources of error affecting their physical precision are discussed in detail in Section 1.9

1.7 Numerical results

Before showing the results which enable to settle the technical and theoretical accuracy of the generators, it is worth discussing the impact of the various sources of radiative corrections implemented in the programs used in the experimental analysis. This allows to understand which corrections are strictly necessary to achieve a precision at the per mille level, for both the calculation of integrated cross section and simulation of more exclusive distributions.

1.7.1 Integrated cross sections

The first set of phenomenological results about radiative corrections refer to the Bhabha cross section, as obtained by means of the code BabaYaga@NLO, according to different perturbative and precision levels. In Tab. 3 we show the values for Born cross section σ_0 , the $\mathcal{O}(\alpha)$ PS and exact cross section, $\sigma_\alpha^{\text{PS}}$ and $\sigma_\alpha^{\text{NLO}}$, respectively, as well as the LL PS cross section σ^{PS} and the matched cross section σ_{exp} . Furthermore, the cross section in the presence of the vacuum polarization correction, $\sigma_{0,\text{VP}}$, is also shown. The results correspond to the c.m. energies $\sqrt{s} = 1, 4, 10$ GeV, and were obtained with the selection criteria of Eq. (12), but for an angular acceptance of $55^\circ \leq \theta_\pm \leq 125^\circ$ resembling realistic data taking at meson factories. It is worth noticing that the cuts of Eq. (12) tend to single out quasi-elastic Bhabha events and that the energy of final-state electron/positron corresponds to a so-called “bare” event selection (i.e. without photon recombination), which corresponds to what is done in practice at flavour factories. In particular, the rather stringent energy and acollinearity cuts enhance the impact of soft and collinear radiation with respect to a more inclusive set up.

From these cross section values, it is possible to calculate the relative effect of various corrections, namely the contribution of vacuum polarization and exact $\mathcal{O}(\alpha)$

QED corrections, of non-logarithmic (NLL) terms entering the $\mathcal{O}(\alpha)$ cross section, of HO corrections in the $\mathcal{O}(\alpha)$ matched PS scheme and, finally, of NNLO effects beyond order α , largely dominated by $\mathcal{O}(\alpha^2 L)$ contributions. The above per cent corrections are shown in Tab. 4 and can be derived from the cross section results of Tab. 3 according to the following definitions

$$\begin{aligned}\delta_{\text{VP}} &\equiv \frac{\sigma_0^{\text{VP}} - \sigma_0}{\sigma_0} & \delta_\alpha &\equiv \frac{\sigma_{\text{NLO}} - \sigma_0}{\sigma_0} \\ \delta_\alpha^{\text{NLL}} &\equiv \frac{\sigma_{\text{NLO}} - \sigma_\alpha^{\text{PS}}}{\sigma_{\text{NLO}}} & \delta_{\text{HO}} &\equiv \frac{\sigma_{\text{matched}} - \sigma_{\text{NLO}}}{\sigma_{\text{NLO}}} \\ \delta_{\alpha^2 L} &\equiv \frac{\sigma_{\text{matched}} - \sigma_\alpha^{\text{NLO}} - \sigma^{\text{PS}} + \sigma_\alpha^{\text{PS}}}{\sigma_0}\end{aligned}$$

From Tab. 4 it can be seen that $\mathcal{O}(\alpha)$ corrections decrease the Bhabha cross section of about 15÷17% at the Φ and τ -charm factories, and of about 20% at the B -factories. Within the full set of $\mathcal{O}(\alpha)$ corrections, non-log terms are of the order of 0.5%, almost independently of the centre-of-mass (c.m.) energy, as expected, and with a mild dependence on the angular acceptance cuts, as due to box/interference contributions. The effect of HO corrections due to multiple photon emission is about 1% at the Φ and τ -charm factories and reaches about 2% at the B -factories. The contribution of (approximate) $\mathcal{O}(\alpha^2 L)$ corrections is at the 0.1% level, while the vacuum polarization increases the cross section of about 2% around 1 GeV, and of about 5% and 6% at 4 GeV and 10 GeV, respectively. Concerning the latter correction, the non-perturbative hadronic contribution to the running of α were parameterized in terms of the HADR5N routine [211, 212], included in BabaYaga@NLO both in the LO and one-loop diagrams. However, during the workshop, we checked that the results obtained for the vacuum polarization correction in terms of the parametrization [120] agree, at the 10^{-4} level, with those obtained with HADR5N, as shown in detail in Section 1.9. It is worth noticing that such routines return a data-driven error, thus affecting the theoretical precision of the calculation of the Bhabha cross section, as discussed, in conclusion, in Section 1.10.

Analogous results about the size of radiative corrections to the process $e^+e^- \rightarrow \gamma\gamma$ are given in Tab. 5 [213]. They were obtained using BabaYaga@NLO, according to the experimental set up of Eq. (13) and for the c.m. energies $\sqrt{s} = 1, 3, 10$ GeV.

The numerical errors coming from the MC integration are not shown in Tab. 4 because they are beyond the quoted digits. From Tab. 4 it can be seen that the exact $\mathcal{O}(\alpha)$ corrections lower the Born cross section of about 5.9% (Φ resonance), 7.0% (at $\sqrt{s} = 3$ GeV) and 8.2% (Υ resonance). The effect due to $\mathcal{O}(\alpha^n L^n)$ (with $n \geq 2$) terms is quantified by the contribution δ_{HO} , which is a positive correction of about 0.2% (Φ resonance), 0.4% (τ -charm factories) and 0.5% (Υ resonance), and, therefore, important in the light of the aimed per mille accuracy. On the other hand, also next-to-leading $\mathcal{O}(\alpha)$ corrections, quantified by the contribution $\delta_\alpha^{\text{NLL}}$, are necessary at the

Table 4. Relative size of different sources of correction (in per cent) to the large-angle Bhabha cross section for typical selection cuts at Φ , τ -charm and B factories.

$\sqrt{s}(\text{GeV})$	1.02	4.	10.
δ_α	-14.73	-17.32	-19.57
$\delta_\alpha^{\text{NLL}}$	-0.66	-0.68	-0.70
δ_{HO}	0.97	1.35	1.79
$\delta_{\alpha^2 L}$	0.09	0.09	0.11
δ_{VP}	2.43	4.46	6.03

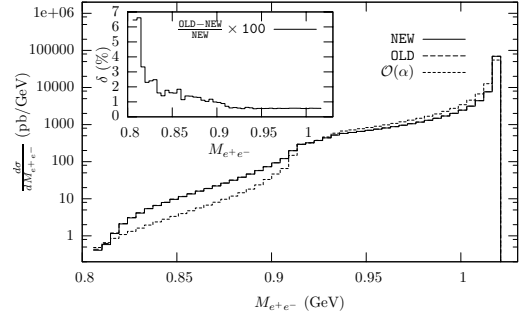
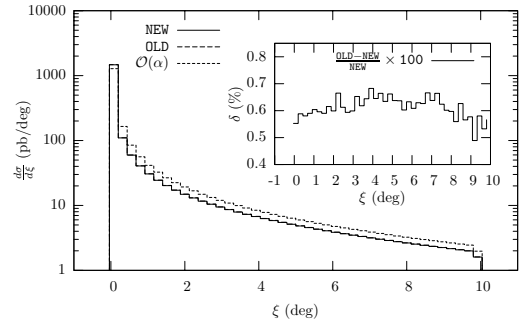
Table 5. Photon pair production cross sections (in nb) to different accuracy levels and relative corrections (in per cent) for the set up of Eq. (13) and the c.m. energies $\sqrt{s} = 1, 3, 10$ GeV.

$\sqrt{s} \text{ (GeV)}$	1	3	10
σ_0	137.53	15.281	1.3753
σ_{NLO}	129.45	14.211	1.2620
$\sigma_\alpha^{\text{PS}}$	128.55	14.111	1.2529
σ_{matched}	129.77	14.263	1.2685
σ^{PS}	128.92	14.169	1.2597
δ_α	-5.87	-7.00	-8.24
$\delta_\alpha^{\text{NLL}}$	0.70	0.71	0.73
δ_{HO}	0.24	0.37	0.51

precision level of 0.1%, since their contribution is of about 0.7%, almost independently of the c.m. energy. To further corroborate the precision reached in the cross section calculation of $e^+e^- \rightarrow \gamma\gamma$, we also evaluated the effect due to the most important sub-leading $\mathcal{O}(\alpha^2)$ photonic corrections and given by $\alpha^2 L$ contributions enhanced by infrared logarithms. It turns out that the effect due to $\mathcal{O}(\alpha^2 L)$ corrections does not exceed the 0.05% level. Obviously, the contribution of vacuum polarization is absent in $\gamma\gamma$ production and this an advantage for particularly precise predictions, as the uncertainty associated to the hadronic part of vacuum polarization does not affect the cross section calculation.

1.7.2 Distributions

Besides the integrated cross section, various differential cross sections are used by the experimental collaborations to monitor the collider luminosity. In Fig. 16 and Fig. 17 we show two distributions which are particularly sensitive to the details of photon radiation, i.e. the e^+e^- invariant mass and acollinearity distribution, in order to quantify the size of NLO and HO corrections. To this end, the distributions obtained according to the exact $\mathcal{O}(\alpha)$ calculation, and the two BabaYaga versions, BabaYaga v3.5 and BabaYaga@NLO, are shown. From Fig. 16 and Fig. 17 it can be clearly seen that multiple photon corrections introduce significant deviations with respect to an $\mathcal{O}(\alpha)$ simulation, especially in the hard tails of the distributions, where they amount to several per cent. To make clearly visible the contribution of exact $\mathcal{O}(\alpha)$ non-log terms, the

**Fig. 16.** Invariant mass distribution of the Bhabha process at KLOE, according to BabaYaga v3.5 (OLD), BabaYaga@NLO (NEW) and an exact NLO calculation. The inset shows the relative effect of NLO corrections, given by the difference of BabaYaga v3.5 and BabaYaga@NLO predictions.**Fig. 17.** Acollinearity distribution of the Bhabha process at KLOE, according to BabaYaga v3.5 (OLD) and BabaYaga@NLO (NEW). The inset shows the relative effect of NLO corrections, given by the difference of BabaYaga v3.5 and BabaYaga@NLO predictions.

inset shows the relative differences between the predictions of BabaYaga v3.5 (denoted as OLD) and BabaYaga@NLO (denoted as NEW). Actually, as discussed in Section 1.5.2, these differences mainly come from non-log NLO contributions and, to a smaller extent, from $\mathcal{O}(\alpha^2 L)$ terms. Their effect is flat and at level of 0.5% for the acollinearity distribution, while they reach the some per cent level in the hard tail of the invariant mass distribution.

It is also worth noticing that LL radiative corrections beyond α^2 can be quite important for accurate simulations, at least when considering differential distributions. This means that, even with a complete NNLO calculation at hand, it would be desirable a matching of such corrections with the resummation of all the remaining LL effects. In Fig. 18, the relative effect of HO corrections beyond α^2 , dominated by α^3 contributions (dashed line), is shown in comparison with that of the α^2 corrections (solid line) on the acollinearity distribution for the Bhabha process at DAΦNE. As it can be seen, the α^3 effect can be as large as 10% in the phase space region of soft photons emission, corresponding to small acollinearity angles with almost back-to-back final-state fermions.

Concerning the process $e^+e^- \rightarrow \gamma\gamma$, in Fig. 19 we show the energy distribution of the most energetic photon, while

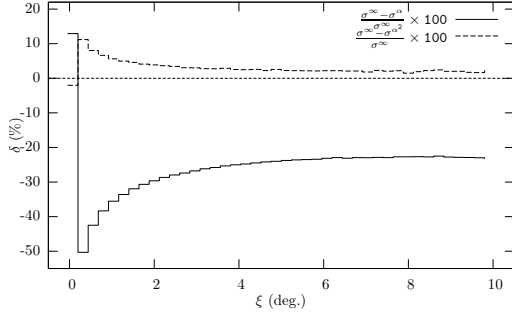


Fig. 18. Relative effect of HO corrections $\alpha^2 L^2$ and $\alpha^n L^n$ ($n \geq 3$) on the acollinearity distribution of the Bhabha process at KLOE.

the acollinearity distribution of the two most energetic photons is represented in Fig. 20. The above distributions refer to exact $\mathcal{O}(\alpha)$ corrections matched with the PS algorithm (solid line), to the exact NLO calculation (dashed line) and to all-order pure PS predictions of BabaYaga v3.5 (dash-dotted line). In the inset of each plot, the relative effect due to multiple photon contributions (δ_{exp}) and non-logarithmic terms entering the improved PS algorithm ($\delta_{\infty}^{\text{NLL}}$) is also shown, according to the definitions given in Eq. (66).

For the energy distribution of the most energetic photon particularly pronounced effects due to exponentiation are present. In the statistically dominant region HO corrections reduce the $\mathcal{O}(\alpha)$ distribution of about 20%, while they give rise to a significant hard tail in the proximity of the energy threshold of $0.3\sqrt{s}$, as a consequence of the higher photon multiplicity of the resummed calculation with respect to the fixed-order NLO prediction. Concerning the acollinearity distribution, the contribution of higher-order corrections is positive and of about 10% in correspondence of quasi back-to-back photon events, whereas it is negative and decreasing from $\sim -30\%$ to $\sim -10\%$ for increasing acollinearity values. As far as the contributions of non-logarithmic effects, dominated by next-to-leading $\mathcal{O}(\alpha)$ corrections, are concerned, they contribute at the level of some per mille for the acollinearity distribution, while they lie in the some per cent range for the energy distribution.

As a whole, the results shown and discussed in the present Section emphasize that both exact $\mathcal{O}(\alpha)$ and HO photonic corrections are necessary, in association with the running of α , for 0.1% theoretical precision, for both cross sections and distributions.

1.8 Tuned comparisons

The typical procedure followed in the literature to establish the technical precision of the theoretical tools is to perform tuned comparisons between the predictions of independent programs, using the same set of input parameters and experimental cuts. This strategy was initiated during the CERN workshops for precision physics at LEP and is still in use nowadays when considering processes of

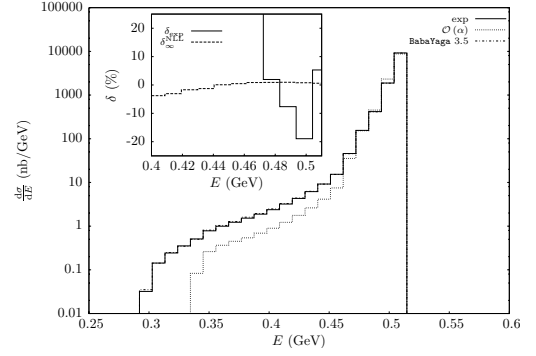


Fig. 19. Energy distribution of the most energetic photon in the process $e^+e^- \rightarrow \gamma\gamma$, according to the PS matched with $\mathcal{O}(\alpha)$ corrections (solid line), the exact $\mathcal{O}(\alpha)$ calculation (dashed line) and the pure all-order PS as in BabaYaga v3.5 (dash-dotted line). Inset: relative effect (in per cent) of multiple photon corrections (solid line) and of non-log contributions of the matched PS algorithm (dashed line).

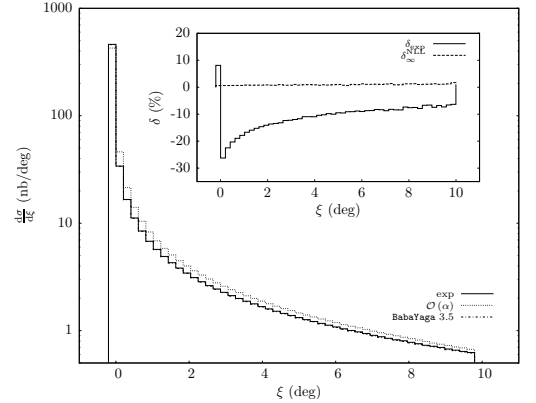


Fig. 20. Acollinearity distribution for the process $e^+e^- \rightarrow \gamma\gamma$, according to the PS matched with $\mathcal{O}(\alpha)$ corrections (solid line), the exact $\mathcal{O}(\alpha)$ calculation (dashed line) and the pure all-order PS as in BabaYaga v3.5 (dash-dotted line). Inset: relative effect (in per cent) of multiple photon corrections (solid line) and of non-log contributions of the matched PS algorithm (dashed line).

interest for physics at hadron colliders, such as single W and Z production, demanding particularly accurate theoretical calculations. The tuning procedure is a key step in the validation of generators, because it allows to check that the different details entering the complex structure of generators themselves, e.g. implementation of radiative corrections, event selection routines, MC integration and event generation, are under control and to fix possible bugs.

The tuned comparisons discussed in the following were performed switching off the vacuum polarization correction to the Bhabha scattering cross section. Actually, the generators implement the non-perturbative hadronic contribution to the running of α according to different parameterizations, which differently affect the cross section prediction. Hence, this simplification is introduced to

avoid possible bias in the interpretation of the results and allows to disentangle the effect of pure QED corrections. Also, the comparisons take into *realistic* event selection cuts, in order to provide results of actual experimental interest.

The present Section is a merge of results available in the literature [186] with those of new studies done during the workshop. The results refer to the Bhabha process at the energies of Φ , τ -charm and B factories. No effort was done on tuned comparisons for the two photon production process.

1.8.1 Φ and τ -charm factories

First, we show comparisons between BabaYaga@NLO and BHWIDE according to the KLOE selection cuts of Eq. (12), but considering in addition also the angular range $20^\circ \geq \vartheta_\pm \leq 160^\circ$ for cross section results. The predictions of the two codes are reported in Tab. 6, for the two acceptance cuts, together with their relative deviations. As can be seen, the agreement is excellent, the relative deviations being well below the 0.1%. Comparisons between BabaYaga@NLO and BHWIDE at the level of differential distributions are given in Fig. 21 and Fig. 22, where the inset shows the relative deviations between the predictions of the two codes. As can be seen, there is a very good agreement between the two generators, as the predicted distributions appear, at a first sight, almost indistinguishable. Looking in more detail, there is a relative difference of a few per mille for the acollinearity distribution (Fig. 22) and of a few per cent for the invariant mass (Fig. 21), but only in the very hard tails, which contribute to the integrated cross section negligibly. In fact, these differences on differential distributions translate into an agreement on the cross section values well below the one per mille, as already shown in Tab. 6.

Similar tuned comparisons were performed during the workshop between the results of BabaYaga@NLO, BHWIDE and MCGPJ in the presence of cuts modeling the event selection criteria of the CMD-2 experiment at the VEPP-2M collider, for a c.m. energy of $\sqrt{s} = 900$ MeV. The cuts used in this case are:

$$\begin{aligned} |\theta_- + \theta_+ - \pi| &\leq \Delta\theta & 1.1 \leq (\theta_+ - \theta_- + \pi)/2 \leq \pi - 1.1 \\ ||\phi_- + \phi_+| - \pi| &\leq 0.15 \\ p_- \sin(\theta_-) &\geq 90 \text{ MeV} & p_+ \sin(\theta_+) \geq 90 \text{ MeV} \\ (p_- + p_+)/2 &\geq 90 \text{ MeV} \end{aligned} \quad (66)$$

where θ_- , θ_+ are the electron/positron polar angles (in radians), respectively, ϕ_\pm their azimuthal angles, and $p_\pm = \sqrt{p_{\pm,x}^2 + p_{\pm,y}^2 + p_{\pm,z}^2}$ the moduli of their three-momenta. $\Delta\theta$ stands for an acollinearity cut.

Fig. 23 shows the relative differences between the results of BHWIDE and MCGPJ according to the criteria of Eq. (66), as a function of the acollinearity cut $\Delta\theta$. The relative deviations between the calculations of BabaYaga@NLO and MCGPJ for the same cuts are given in Fig. 24. It can be seen that the predictions of the three generators lie

Table 6. Cross section predictions [nb] of BabaYaga@NLO and BHWIDE for the Bhabha cross section corresponding to two different angular acceptances, for KLOE experiment at DAΦNE, and their relative differences.

angular acceptance	BabaYaga@NLO	BHWIDE	$\delta(\%)$
$20^\circ \div 160^\circ$	6086.6(1)	6086.3(2)	0.005
$55^\circ \div 125^\circ$	455.85(1)	455.73(1)	0.030

Table 7. Cross section predictions [nb] of BabaYaga@NLO and MCGPJ for the Bhabha cross section at τ -charm factories and their relative difference.

BabaYaga@NLO	MCGPJ	$\delta(\%)$
35.20(2)	35.181(5)	0.06

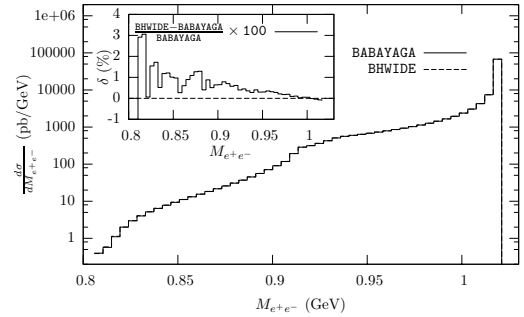


Fig. 21. Invariant mass distribution of the Bhabha process according to BHWIDE and BabaYaga@NLO, for KLOE experiment at DAΦNE, and relative differences of the codes predictions (inset).

within a 0.2% band, with differences of $\sim 0.3\%$ for extreme values of the acollinearity cut only. This agreement can be considered certainly satisfactory, since for the acollinearity cuts of real interest the generators agree at the one per mille.

A number of comparisons was also performed for a c.m. energy of 3.5 GeV relevant for experiments at τ -charm factories. An example is given in Tab. 7, where the predictions of BabaYaga@NLO and MCGPJ are compared, using cuts similar to those of Eq. (66), for an acollinearity cut $\Delta\theta = 0.25$ rad. As it can be seen, the agreement between the two codes is below the one per mille. Comparisons between the two codes were also done at the level of differential cross sections, showing satisfactory agreement in the statistically relevant phase-space regions. Preliminary results [214] for a c.m. energy on top of the J/ψ resonance show good agreement between BabaYaga@NLO and BHWIDE predictions too.

1.8.2 B -factories

Concerning the B -factories, a considerable effort was done to establish the level of agreement between BabaYaga@NLO

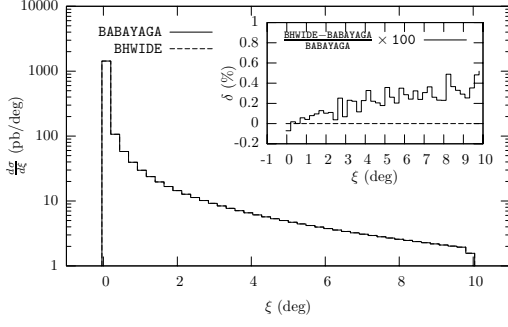


Fig. 22. Acollinearity distribution of the Bhabha process according to BHWIDE and BabaYaga@NLO, for KLOE experiment at DAΦNE, and relative differences of the codes predictions (inset).

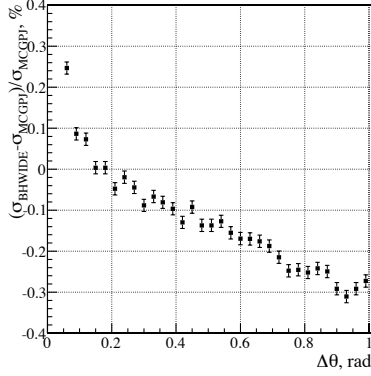


Fig. 23. Relative differences between BHWIDE and MCGPJ Bhabha cross sections as a function of the acollinearity cut, for CMD-2 experiment at VEPP-2M.

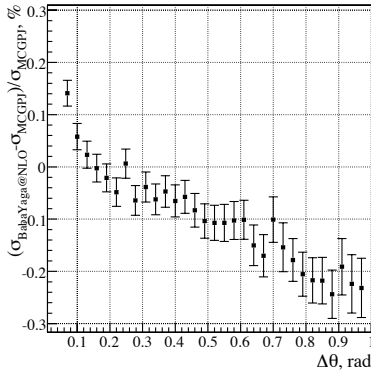


Fig. 24. Relative differences between BabaYaga@NLO and MCGPJ Bhabha cross sections as a function of the acollinearity cut, for CMD-2 experiment at VEPP-2M.

Table 8. Cross section predictions [nb] of BabaYaga@NLO and BHWIDE for the Bhabha cross section as a function of the angular selection cuts, for Babar experiment at PEP-II, and their relative differences.

angular range (c.m.s.)	BabaYaga@NLO	BHWIDE	$\delta(\%)$
$15^\circ \div 165^\circ$	119.5(1)	119.53(8)	0.025
$30^\circ \div 150^\circ$	24.17(2)	24.22(2)	0.207
$40^\circ \div 140^\circ$	11.67(3)	11.660(8)	0.086
$50^\circ \div 130^\circ$	6.31(3)	6.289(4)	0.332
$60^\circ \div 120^\circ$	1.928(2)	1.931(3)	0.141
$70^\circ \div 110^\circ$	3.554(6)	3.549(3)	0.155
$80^\circ \div 100^\circ$	0.824(2)	0.822(1)	0.243

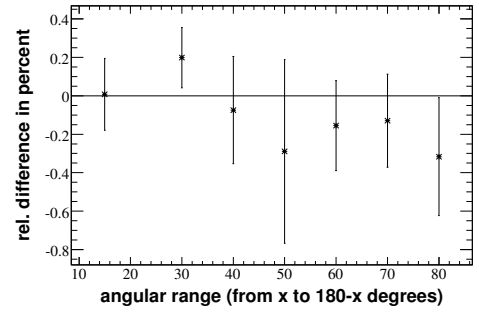


Fig. 25. Relative differences between BabaYaga@NLO and BHWIDE Bhabha cross sections as a function of the angular acceptance cut, for the Babar experiment at PEP-II.

and BHWIDE, in comparison with BabaYaga v3.5 too. This study made use of the realistic luminosity cuts quoted in Section 1.4.3 for the Babar experiment. The cross sections predicted by BabaYaga@NLO and BHWIDE are shown in Tab. 8, together with the corresponding relative differences, as a function of the considered angular range. To guide the eye, the latter are also shown in Fig. 25, where the 1σ numerical error due to MC statistics are also quoted. As can be seen, the two codes nicely agree, the central value predictions being, in general, in agreement at the 0.1% level or statistically compatible whenever a two-three per mille difference is present.

To further investigate how the two generators compare, a number of differential cross sections was studied. The results of this study are shown in Fig. 26 and Fig. 27, for the electron energy and polar angle distribution, respectively, and in Fig. 28 for the acollinearity distributions. For both the energy and scattering angle distribution, the two programs agree within the statistical errors, showing deviations, if present, not above the 0.5%. For the acollinearity dependence of the cross section, BabaYaga@NLO and BHWIDE agree within $\sim 1\%$. Therefore, the level of the agreement between the two codes around 10 GeV is the same as that observed at the Φ factories.

The main conclusions emerging from the tuned comparisons discussed in the present Section can be summarized as follows:

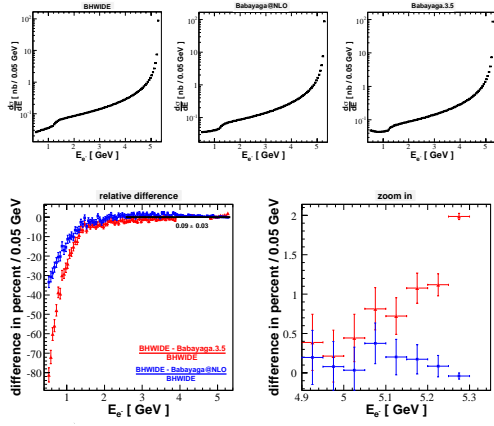


Fig. 26. Electron energy distributions according to BHWIDE, BabaYaga@NLO and BabaYaga v3.5 for the Babar experiment at PEP-II, and relative differences of the codes predictions.

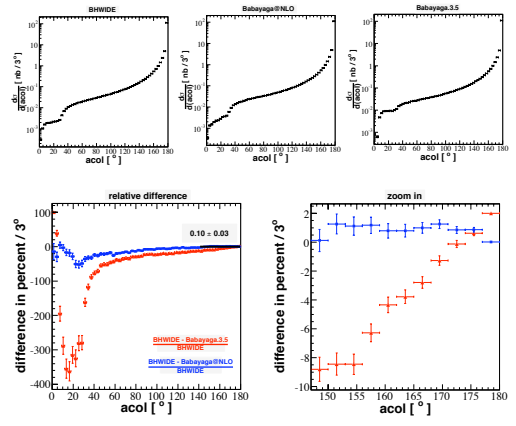


Fig. 28. Acollinearity distributions according to BHWIDE, BabaYaga@NLO and BabaYaga v3.5 for the Babar experiment at PEP-II, and relative differences of the codes predictions.

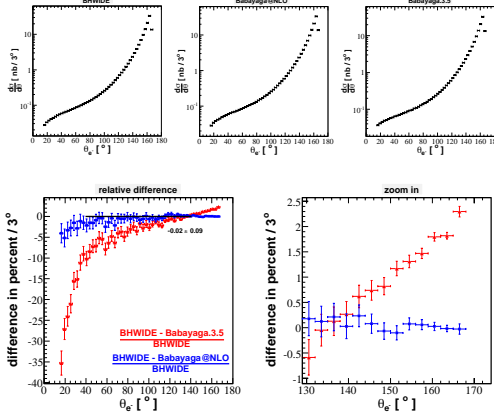


Fig. 27. Electron polar angle distributions according to BHWIDE, BabaYaga@NLO and BabaYaga v3.5 for the Babar experiment at PEP-II, and relative differences of the codes predictions.

- The predictions for the Bhabha cross section of the mostly precise tools, i.e. BabaYaga@NLO, BHWIDE and MCGPJ, generally agree within 0.1%. If (slightly) larger differences are present, they show up for particularly severe cuts or are due to limited MC statistics. When statistically meaningful discrepancies are observed, they can be ascribed to the different theoretical recipes for the treatment of radiative corrections and their technical implementation. However, such differences are definitely small in comparison with the typical experimental error.
- Also the distributions predicted by the generators agree well, with relative differences below the 1% level. Slightly larger discrepancies are only seen in sparse populated phase-space regions corresponding to very hard pho-

ton emission and which do not influence the luminosity measurement.

1.9 Theoretical accuracy

As discussed in Section 1.1, the total luminosity error crucially depends on the theoretical accuracy of the generators used by the experimental collaborations. As emphasized in Section 1.6, some of these programs, i.e. Bagenf, BabaYaga v3.5 and BKQED, miss theoretical ingredients which are unavoidable for cross section calculation with a precision at the per mille level. Therefore, they are inadequate for a highly accurate luminosity determination. On the other hand, BabaYaga@NLO, BHWIDE and MCGPJ include both NLO and multiple photon corrections and, as such, their accuracy aims at a precision of 0.1%. However, also the above generators are affected by uncertainties which must carefully considered in the light of the very stringent criteria of per mille physics. The most important components of the theoretical error of BabaYaga@NLO, BHWIDE and MCGPJ come from the following sources:

1. the non-perturbative light quarks contribution to the running of α . It can be reliably evaluated only using the data of the hadron cross section at low energies. Hence, the vacuum polarization correction receives a data-driven error, which affects, in turn, the prediction of the Bhabha cross section.
2. the complete set of $\mathcal{O}(\alpha^2)$ QED corrections. In spite of the impressive progress in this area, as reviewed in Section 1.4, an important piece of NNLO corrections, i.e. exact NLO SV corrections to the single hard bremsstrahlung process $e^+e^- \rightarrow e^+e^-\gamma$, is still missing for the full $s+t$ Bhabha process. However, partial results obtained for t -channel small-angle Bhabha scattering [215, 216] and large-angle annihilation processes are available [217, 218].

3. the $\mathcal{O}(\alpha^2)$ contribution due to real and virtual (lepton and hadron) pairs. The virtual contributions originate from the NNLO electron, heavy flavor and hadronic loop corrections discussed in Section 1.4, while the real corrections are due to the conversion of a photon into pairs. The latter, as discussed in Section 1.4.3, gives rise to a final state with four particles, two of which to be considered as undetected to contribute to the Bhabha signature.

The uncertainty relative to point 1. can be estimated by using the routines available in the literature for the calculation of the non-perturbative hadronic contribution $\Delta\alpha_{\text{hadr}}^{(5)}(q^2)$ to the vacuum polarization. Actually, these routines return, in addition to $\Delta\alpha_{\text{hadr}}^{(5)}(q^2)$, an error δ_{hadr} on its value. Therefore, an estimate of the induced error can be simply obtained by computing the Bhabha cross section with $\Delta\alpha_{\text{hadr}}^{(5)}(q^2) \pm \delta_{\text{hadr}}$ and taking the difference as the theoretical uncertainty due to the hadronic contribution to vacuum polarization. In Tab. 9, the Bhabha cross sections, as obtained in the presence of the vacuum polarization correction according to the parameterization of [211, 212] (denoted as J) and of [120] (denoted as HMNT), respectively, are shown for Φ , τ -charm and B factories. The applied angular cuts refer to the typically adopted acceptance $55^\circ \leq \theta_{\pm} \leq 125^\circ$.

Table 9. Bhabha scattering cross section in the presence of the vacuum polarization correction, according to [211, 212] (J) and [120] (HMNT), at meson factories. The notation J₋/HMNT₋, J/HMNT and J₊/HMNT₊ indicates minimum, central and maximum value of the two parametrizations.

Parametrization	Φ	τ -charm	B
J ₋	542.662(4)	46.9600(1)	5.85364(2)
J	542.662(4)	46.9658(1)	5.85529(2)
J ₊	542.662(4)	46.9715(1)	5.85693(2)
HMNT ₋	542.500(5)	46.9580(1)	5.85496(1)
HMNT	542.391(5)	46.9638(1)	5.85621(1)
HMNT ₊	542.283(5)	46.9697(1)	5.85746(2)

From Tab. 9 it can be seen that the two treatments of $\Delta\alpha_{\text{hadr}}^{(5)}(q^2)$ induce effects on the Bhabha cross section in very good agreement, the relative differences between the central values being 0.05% (Φ -factories), 0.005% (τ -charm factories) and 0.02% (B -factories). This can be understood in terms of the dominance of t -channel exchange for large-angle Bhabha at meson factories. Indeed, the two routines provide results in excellent agreement for space-like momenta, as we explicitly checked, whereas different predictions show up for time-like momenta, which, however, contribute to the Bhabha cross section very marginally. Also, the spread between the minimum/maximum values and the central one as returned by the two routines agrees very well, because of the same reason just discussed. This spread amounts to a few units in 10^{-4} and is detailed in Tab. 10 in the next Section.

Concerning point 2., a general strategy to evaluate the size of missing NNLO corrections consists in deriving from the theoretical formulation implemented in the generator of interest a cross section expansion up to $\mathcal{O}(\alpha^2)$. It can be cast, in general, in the following form

$$\sigma^{\alpha^2} = \sigma_{\text{SV}}^{\alpha^2} + \sigma_{\text{SV,H}}^{\alpha^2} + \sigma_{\text{HH}}^{\alpha^2} \quad (67)$$

where, in principle, each of the above $\mathcal{O}(\alpha^2)$ contributions is affected by an uncertainty, to be properly estimated. In Eq. (67), the first contribution is the cross section including $\mathcal{O}(\alpha^2)$ soft plus virtual corrections, whose uncertainty can be evaluated through a comparison with some of the available NNLO calculations reviewed in Section 1.4. In particular, in [186] the $\sigma_{\text{SV}}^{\alpha^2}$ of the BabaYaga@NLO generator was compared with the calculation of photonic corrections by Penin [91, 92] and the calculations by Bonciani *et al.* [96, 97, 105, 106, 107], who computed two-loop fermionic corrections (in the one-family approximation $N_F = 1$) with finite mass terms and the addition of soft bremsstrahlung and real pair contributions⁸. The results of such comparisons are shown in Fig. 1.9 and Fig. 30 for realistic cuts at the Φ -factories. In Fig. 1.9 $\delta\sigma$ is the difference between $\sigma_{\text{SV}}^{\alpha^2}$ of BabaYaga@NLO and the cross sections of the two $\mathcal{O}(\alpha^2)$ calculations, denoted as photonic (Penin) and $N_F = 1$ (Bonciani *et al.*), as a function of the logarithm of the infrared regulator ϵ . It can be seen that the differences are given by flat functions, demonstrating that such differences are infrared-safe, as expected, as a consequence of the universality and factorization properties of the infrared divergences. In Fig. 30, $\delta\sigma$ is shown as a function of the logarithm of a fictitious electron mass and for a fixed value of $\epsilon = 10^{-5}$. Since the difference with the calculation by Penin is given by a straight line, this indicates that the soft plus virtual two-loop photonic corrections missing in BabaYaga@NLO are $\mathcal{O}(\alpha^2 L)$ contributions, as already remarked. On the other hand, the difference with the calculation by Bonciani *et al.* is fitted by a quadratic function, showing that the electron two-loop effects missing in BabaYaga@NLO are of the order of $\alpha^2 L^2$. However, it is important to emphasize that, as shown in detail in [186], the sum of the differences with the two $\mathcal{O}(\alpha^2)$ calculations does not exceed the 2×10^{-4} level, for various set up at Φ - and B -factories.

The second term in Eq. (67) is the cross section containing the one-loop corrections to single hard bremsstrahlung and its uncertainty can be estimated by relying on partial results existing in the literature. Actually, the exact perturbative expression of $\sigma_{\text{SV,H}}^{\alpha^2}$ is not available yet for full $s + t$ Bhabha scattering, but, using the results valid for small-angle Bhabha scattering [215, 216] and large-angle s -channel processes [217, 218], the relative uncertainty of the theoretical tools in the calculation of $\sigma_{\text{SV,H}}^{\alpha^2}$ can be conser-

⁸ To provide meaningful results, the contribution of the vacuum polarization was switched off in BabaYaga@NLO to compare with the calculation by Penin consistently. For a similar reason, the real and virtual pair corrections, not implemented in BabaYaga@NLO, were neglected in the comparison with the calculation by Bonciani *et al.*

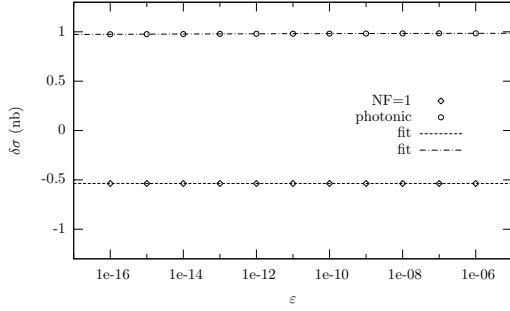


Fig. 29. Relative differences between the $\sigma_{\text{SV}}^{\alpha^2}$ of BabaYaga@NLO and the $\mathcal{O}(\alpha^2)$ calculations of [91,92] (photonic) and of [96,97,105,106,107] ($N_F = 1$), as a function of the infrared regulator ϵ .

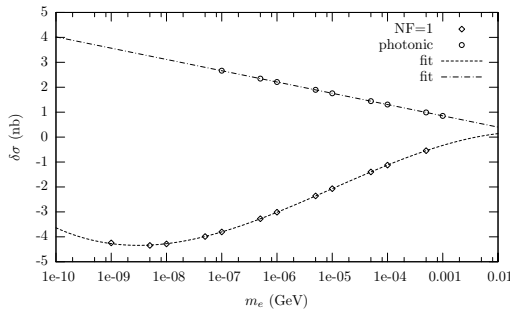


Fig. 30. Relative differences between the $\sigma_{\text{SV}}^{\alpha^2}$ of BabaYaga@NLO and the $\mathcal{O}(\alpha^2)$ calculations of [91,92] (photonic) and of [96,97,105,106,107] ($N_F = 1$), as a function of a fictitious electron mass.

vatively estimated at the level of 0.05%. Indeed, the papers above show that a YFS matching of NLO and HO corrections give SV one-loop results for the t -channel process $e^+e^- \rightarrow e^+e^-\gamma$ and s -channel annihilation $e^+e^- \rightarrow f\bar{f}\gamma$ ($f = \text{fermion}$) differing from the exact perturbative calculations for a few units in 10^{-4} at most. This conclusion holds when varying applied photon energy cuts.

The third contribution in Eq. (67) is the double hard bremsstrahlung cross section, whose uncertainty can be directly evaluated by explicit comparison with the exact $e^+e^- \rightarrow e^+e^-\gamma\gamma$ cross section. In [186], it was shown that the differences between $\sigma_{\text{HH}}^{\alpha^2}$ as in BabaYaga@NLO and the matrix element calculation, which exactly describes the contribution of two hard photons, are really negligible, at the 10^{-5} level.

The relative effect due lepton (e, μ, τ) and hadron (π) pairs has been numerically analyzed in Section 1.4.3, in the presence of realistic selection cuts. This evaluation makes use of the complete NNLO virtual corrections in association with an exact matrix element calculation of the four-particle production processes. It represents an original contribution to the workshop and supersedes previous approximate estimates, which underestimated the impact of such corrections. According to this new evaluation, the pair contribution, dominated by the electron pair correc-

tion, amounts, in particular, to about 0.05% at KLOE and 0.25% at Babar.

1.10 Conclusions and open issues

During the last few years, a remarkable progress occurred in reducing the error associated to the luminosity measurement at flavour factories. These advances were presented between the workshop, together with original work towards more and more reliable theoretical predictions and a better control of the technical precision of the analysis tools.

Dedicated event generators, namely BabaYaga@NLO and MCGPJ, were developed to provide predictions for the cross section of the large-angle Bhabha process, as well as the other QED reactions of interest, with a theoretical accuracy at the level of 0.1%. In parallel, codes well-known since the time of LEP/SLC operation, such as BHWIDE, were taken into consideration by the experiments and extensively used in data analysis. These MC programs all include, albeit according to different formulations, exact $\mathcal{O}(\alpha)$ corrections matched with LL contributions coming from multiple photon emission. Such ingredients, together with the vacuum polarization correction, are strictly necessary to achieve a physical precision down to the per mille level. Indeed, when considering typical selection cuts, the NLO photonic corrections amount to about 15÷20%, the vacuum polarization contributes at the some per cent level and HO effects lie between 1÷2%.

On the other hand, the generators above are affected by an uncertainty due to those HO effects neglected in their formulation, such as light pair corrections or exact perturbative contributions present in NNLO calculations. From this point of view, the great progress in the calculation of two-loop corrections to the Bhabha scattering cross section was essential to establish the theoretical accuracy of the existing generators and is crucial if an improvement of the precision below the one per mille will be required.

During the workshop, a particular effort was done to compare the generators predictions consistently, in order to assess the technical precision in the implementation of radiative corrections and related computational details. These comparisons were performed in the presence of realistic event selection criteria, and at different c.m. energies. For the experiments KLOE and CMD-2 around the Φ -resonance, where the statistics of Bhabha events is the highest and the experimental luminosity error at a few mille level, the cross section results of BabaYaga@NLO, BHWIDE and MCGPJ agree within $\sim 0.1\%$. If (slightly) larger discrepancies are observed, they show up only for particularly severe cuts or exclusive distributions in specific phase-space region, which do not influence the luminosity determination. Very similar results were obtained for τ -charm and B -factories. The main conclusion of the work on tuned comparisons is that the technical precision of MC programs is well under control, the discrepancies (whenever present) being definitely smaller than the experimental error.

On the theoretical side, a new, exact evaluation of lepton and hadron pair corrections to the Bhabha scattering cross section was carried out, taking into account realistic cuts. This calculation provides results in rough agreement with estimates based on singlet SF, but supersedes previous evaluations in the soft-photon approximation. Also, the contribution induced by the uncertainty associated to non-perturbative contribution to the running of α was revisited, making use of and comparing the two independent parameterizations derived in [211, 212] and [120].

A summary of the different sources of theoretical error and their relative impact on the Bhabha cross section is given in Tab. 10. In this Table, $|\delta_{\text{VP}}^{\text{err}}|$ is the error induced by the hadronic component of the vacuum polarization, $|\delta_{\text{pairs}}^{\text{err}}|$ the error due to missing pair corrections, $|\delta_{\text{SV}}^{\text{err}}|$ the uncertainty coming from SV NNLO corrections, $|\delta_{\text{HH}}^{\text{err}}|$ the uncertainty in the calculation of the double hard bremsstrahlung process and $|\delta_{\text{SV,H}}^{\text{err}}|$ the error estimate for one-loop corrections to single hard bremsstrahlung. As it can be seen, pair corrections and exact NLO corrections to $e^+e^- \rightarrow e^+e^-\gamma$ are the dominant sources of error.

The total theoretical uncertainty, as obtained by summing the different contributions linearly, is $0.12 \div 0.14\%$ at the Φ factories, 0.18% at the τ -charm factories and $\sim 0.35\%$ at the B factories. This uncertainty is slightly affected by the particular choice of the routine for the calculation of $\Delta\alpha_{\text{hadr}}^{(5)}(q^2)$, since the two parametrizations considered here give rise to similar errors, with the exception of the Φ -factories for which the two recipes return uncertainties differing of 2×10^{-4} . However, as remarked in [186], the hadronic contribution to vacuum polarization becomes a relevant source of uncertainty, at some per mille level, when considering predictions for a c.m. energy exactly on top of the J/Ψ resonance. For such a specific situation, of interest, for instance, for the BES experiment, the two prescriptions for $\Delta\alpha_{\text{hadr}}^{(5)}(q^2)$ differ significantly because of the quite different description of narrow resonances. For the time being, in the absence of new data around the J/Ψ , the error driven by $\Delta\alpha_{\text{hadr}}^{(5)}(q^2)$ in this energy region is an irreducible limiting factor and deteriorates the total uncertainty in the Bhabha cross section prediction up to several per mille.

The theoretical uncertainty quoted in Tab. 10 is sufficient for present and planned precision luminosity measurements at meson factories, the experimental error currently being about a factor of two or three larger than such an accuracy. Adopting the strategy followed during LEP/SLC operation for the luminosity theoretical budget, one could arrive at a more aggressive error estimate, by summing the relative contributions in quadrature. However, for the time being, this does not seem to be necessary in the light of the current experimental error.

It is worth noticing, in conclusion, that the precision presently reached by large-angle Bhabha programs used in the luminosity measurement at meson factories is comparable, especially at the Φ -factories, with that achieved about ten years ago for luminosity monitoring through small-angle Bhabha scattering at LEP/SLC.

Table 10. Summary of different sources of theoretical uncertainty in the most precise generators used in the luminosity measurement, and corresponding total theoretical error for the calculation of the large-angle Bhabha cross section at meson factories.

Source of error (%)	Φ	τ -charm	B
$ \delta_{\text{VP}}^{\text{err}} $ [211, 212]	0.00	0.01	0.03
$ \delta_{\text{VP}}^{\text{err}} $ [120]	0.02	0.01	0.02
$ \delta_{\text{pairs}}^{\text{err}} $	0.05	0.1 ⁹	0.25
$ \delta_{\text{SV}}^{\text{err}} $	0.02	0.02	0.02
$ \delta_{\text{HH}}^{\text{err}} $	0.00	0.00	0.00
$ \delta_{\text{SV,H}}^{\text{err}} $	0.05	0.05	0.05
$ \delta_{\text{total}}^{\text{err}} $	$0.12 \div 0.14$	0.18	$0.34 \div 0.35$

The work done during the workshop left open some issues. In the context of tuned comparisons, no effort was done to compare the available codes for the process of photon pair production. Since it contributes relevantly to the luminosity determination and precise predictions for its cross section can be obtained through the codes BabaYaga@NLO and MCGPJ, this work should be done, soon or later. This would lead to a deeper understanding of luminosity on the experimental side. In the framework of new theoretical advances, an evaluation of the light pair contribution to the process $e^+e^- \rightarrow \gamma\gamma$ would be helpful to better assess the precision of the generators which include, for the time being, only photonic corrections to such a process. More importantly, the exact one-loop corrections to the radiative process $e^+e^- \rightarrow e^+e^-\gamma$ should be calculated, going beyond the partial results scattered in the literature (and referring to selection criteria valid for high-energy e^+e^- colliders) or limited to the soft-photon approximation. This contribution should be evaluated taking into account the experimental cuts used at meson factories, to get a better control of the theoretical uncertainty in the sector of NNLO corrections to Bhabha scattering. Incidentally, this calculation would be also of interest for other studies at e^+e^- of moderately high energy, such as the search for new physics phenomena (e.g. dark matter candidates), for which radiative Bhabha scattering is a very important background.

Acknowledgments

The work here presented was partially supported by the INTAS project Nr 05-1000008-8328 “Higher-order effects in e^+e^- annihilation and muon anomalous magnetic moment”. We thank J. Libby for useful correspondence about the luminosity measurement at CLEO-c. We are grateful to T. Teubner for providing us with the routine for the evaluation of the hadronic contribution to vacuum polarization according to HMNT parametrization. Useful discussions with S. Eidelman, F. Jegerlehner, G. Fedotovitch, G. Venanzoni ... ? others ... to be included by all of who, if any are gratefully acknowledged.

References

1. N. Cabibbo and R. Gatto, *Phys. Rev.* 124 (1961) 1577–1595.
2. H. Bhabha, *Proc. Roy. Soc.* A154 (1936) 195.
3. G. Barbiellini et al., *Nucl. Instrum. Meth.* 123 (1975) 125.
4. H. C. Dehne, M. A. Preger, S. Tazzari, and G. Vignola, *Nucl. Instrum. Meth.* 116 (1974) 345–359.
5. S. Jadach et al., [hep-ph/9602393](#).
6. A. Arbuzov et al., *Phys. Lett.* B383 (1996) 238–242, [hep-ph/9605239](#).
7. G. Montagna, O. Nicrosini, and F. Piccinini, *Riv. Nuovo Cim.* 21N9 (1998) 1–162, [hep-ph/9802302](#).
8. S. Jadach, [hep-ph/0306083](#).
9. KLOE Collaboration, F. Ambrosino et al., *Eur. Phys. J.* C47 (2006) 589–596, [hep-ex/0604048](#).
10. CLEO Collaboration, S. Dobbs et al., *Phys. Rev.* D76 (2007) 112001, [0709.3783](#).
11. A. Hafner, [Diploma Thesis, Univ. of Karlsruhe](#).
12. L. M. Brown and R. P. Feynman, *Phys. Rev.* 85 (1952) 231.
13. F. Redhead, *Proc. Roy. Soc.* 220 (1953) 219.
14. R. Polovin, *JETP* 31 (1956) 449.
15. M. Consoli, *Nucl. Phys.* B160 (1979) 208.
16. M. Böhm, A. Denner, W. Hollik, and R. Sommer, *Phys. Lett.* B144 (1984) 414.
17. D. Bardin, W. Hollik, and T. Riemann, *Z. Phys.* C49 (1991) 485–490.
18. D. Bardin, P. Christova, M. Jack, L. Kalinovskaya, A. Olchevski, S. Riemann, and T. Riemann, *Comput. Phys. Commun.* 133 (2001) 229–395, [hep-ph/9908433](#).
19. A. Arbuzov, M. Awramik, M. Czakon, A. Freitas, M. Grünewald, K. Mönig, S. Riemann, and T. Riemann, *Comput. Phys. Commun.* 174 (2006) 728–758, [hep-ph/0507146](#).
20. G. Montagna, F. Piccinini, O. Nicrosini, G. Passarino, and R. Pittau, *Nucl. Phys.* B401 (1993) 3–66.
21. G. Montagna, F. Piccinini, O. Nicrosini, G. Passarino, and R. Pittau, *Comput. Phys. Commun.* 76 (1993) 328–360.
22. G. Montagna, O. Nicrosini, F. Piccinini, and G. Passarino, *Comput. Phys. Commun.* 117 (1999) 278–289, [hep-ph/9804211](#).
23. A. Djouadi and C. Verzegnassi, *Phys. Lett.* B195 (1987) 265.
24. A. Djouadi, *Nuovo Cim.* A100 (1988) 357.
25. B. A. Kniehl, J. H. Kuhn, and R. G. Stuart, *Phys. Lett.* B214 (1988) 621.
26. J. J. van der Bij and F. Hoogeveen, *Nucl. Phys.* B283 (1987) 477.
27. R. Barbieri, M. Beccaria, P. Ciafaloni, G. Curci, and A. Vicere, *Nucl. Phys.* B409 (1993) 105–127.
28. J. Fleischer, O. V. Tarasov, and F. Jegerlehner, *Phys. Lett.* B319 (1993) 249–256.
29. J. Fleischer, O. V. Tarasov, and F. Jegerlehner, *Phys. Rev.* D51 (1995) 3820–3837.
30. R. Boughezal and M. Czakon, *Nucl. Phys.* B755 (2006) 221–238, [hep-ph/0606232](#).
31. K. G. Chetyrkin, M. Faisst, J. H. Kuhn, P. Maierhofer, and C. Sturm, *Phys. Rev. Lett.* 97 (2006) 102003, [hep-ph/0605201](#).
32. Y. Schroder and M. Steinhauser, *Phys. Lett.* B622 (2005) 124–130, [hep-ph/0504055](#).
33. K. G. Chetyrkin, J. H. Kuhn, and M. Steinhauser, *Phys. Lett.* B351 (1995) 331–338, [hep-ph/9502291](#).
34. K. G. Chetyrkin, J. H. Kuhn, and M. Steinhauser, *Phys. Rev. Lett.* 75 (1995) 3394–3397, [hep-ph/9504413](#).
35. R. Barbieri, M. Beccaria, P. Ciafaloni, G. Curci, and A. Vicere, *Phys. Lett.* B288 (1992) 95–98, [hep-ph/9205238](#).
36. J. J. van der Bij, K. G. Chetyrkin, M. Faisst, G. Jikia, and T. Seidensticker, *Phys. Lett.* B498 (2001) 156–162, [hep-ph/0011373](#).
37. M. Faisst, J. H. Kuhn, T. Seidensticker, and O. Veretin, *Nucl. Phys.* B665 (2003) 649–662, [hep-ph/0302275](#).
38. R. Boughezal, J. B. Tausk, and J. J. van der Bij, *Nucl. Phys.* B713 (2005) 278–290, [hep-ph/0410216](#).
39. R. Boughezal, J. B. Tausk, and J. J. van der Bij, *Nucl. Phys.* B725 (2005) 3–14, [hep-ph/0504092](#).
40. M. Awramik, M. Czakon, A. Freitas, and G. Weiglein, *Phys. Rev.* D69 (2004) 053006, [hep-ph/0311148](#).
41. M. Awramik, M. Czakon, A. Freitas, and G. Weiglein, *Phys. Rev. Lett.* 93 (2004) 201805, [hep-ph/0407317](#).
42. W. Hollik, U. Meier, and S. Uccirati, *Nucl. Phys.* B731 (2005) 213–224, [hep-ph/0507158](#).
43. W. Hollik, U. Meier, and S. Uccirati, *Nucl. Phys.* B765 (2007) 154–165, [hep-ph/0610312](#).
44. M. Awramik, M. Czakon, and A. Freitas, *JHEP* 11 (2006) 048, [hep-ph/0608099](#).
45. M. Awramik, M. Czakon, and A. Freitas, *Phys. Lett.* B642 (2006) 563–566, [hep-ph/0605339](#).
46. J. H. Kuhn, A. A. Penin, and V. A. Smirnov, *Eur. Phys. J.* C17 (2000) 97–105, [hep-ph/9912503](#).
47. J. H. Kuhn, A. A. Penin, and V. A. Smirnov, *Nucl. Phys. Proc. Suppl.* 89 (2000) 94–99, [hep-ph/0005301](#).
48. J. H. Kuhn, S. Moch, A. A. Penin, and V. A. Smirnov, *Nucl. Phys.* B616 (2001) 286–306, [hep-ph/0106298](#).
49. B. Feucht, J. H. Kuhn, A. A. Penin, and V. A. Smirnov, *Phys. Rev. Lett.* 93 (2004) 101802, [hep-ph/0404082](#).
50. B. Jantzen, J. H. Kuhn, A. A. Penin, and V. A. Smirnov, *Phys. Rev.* D72 (2005) 051301, [hep-ph/0504111](#).
51. B. Jantzen, J. H. Kuhn, A. A. Penin, and V. A. Smirnov, *Nucl. Phys.* B731 (2005) 188–212, [hep-ph/0509157](#).
52. A. Denner, B. Jantzen, and S. Pozzorini, *Nucl. Phys.* B761 (2007) 1–62, [hep-ph/0608326](#).
53. A. Denner, B. Jantzen, and S. Pozzorini, [0801.2647](#).
54. F. Berends, K. Gaemers, and R. Gastmans, *Nucl. Phys.* B68 (1974) 541.
55. W. Beenakker, F. Berends, and S. van der Marck, *Nucl. Phys.* B349 (1991) 323.
56. M. Terentyev, *Yad. Fiz.* 9 (1969) 1212.
57. F. Berends and R. Gastmans, *Nucl. Phys.* B61 (1973) 414.
58. S. Eidelman and E. Kuraev, *Nucl. Phys.* B143 (1978) 353.
59. F. Berends, R. Kleiss, P. De Causmaecker, R. Gastmans, W. Troost, and T. Wu, *Nucl. Phys.* B206 (1982) 61.
60. M. Böhm and Z. Sack, *Z. Phys.* C33 (1986) 157.
61. S. Laporta and E. Remiddi, *Phys. Lett.* B379 (1996) 283–291, [hep-ph/9602417](#).
62. S. Laporta, *Int. J. Mod. Phys.* A15 (2000) 5087–5159, [hep-ph/0102033](#).
63. F. V. Tkachov, *Phys. Lett.* B100 (1981) 65–68.

64. K. Chetyrkin and F. Tkachov, Nucl. Phys. B192 (1981) 159–204.
65. A. V. Kotikov, Phys. Lett. B254 (1991) 158–164, note.
66. A. Kotikov, Phys. Lett. B259 (1991) 314–322.
67. A. V. Kotikov, Phys. Lett. B267 (1991) 123–127.
68. E. Remiddi, Nuovo Cim. A110 (1997) 1435–1452, [hep-th/9711188](#).
69. M. Caffo, H. Czyz, S. Laporta, and E. Remiddi, Acta Phys. Polon. B29 (1998) 2627–2635, <http://arXiv.org/abs/hep-th/9807119>.
70. M. Caffo, H. Czyz, S. Laporta, and E. Remiddi, Nuovo Cim. A111 (1998) 365–389, <http://arXiv.org/abs/hep-th/9805118>.
71. M. Argeri and P. Mastrolia, Int. J. Mod. Phys. A22 (2007) 4375–4436, [0707.4037](#).
72. V. Smirnov, “Evaluating Feynman Integrals” (Springer Verlag, Berlin, 2004).
73. S. Friot, D. Greynat, and E. De Rafael, Phys. Lett. B628 (2005) 73–84, [hep-ph/0505038](#).
74. N. Usyukina, Teor. Mat. Fiz. 22 (1975) 300–306 (in Russian).
75. V. Smirnov, Phys. Lett. B460 (1999) 397–404, [hep-ph/9905323](#).
76. B. Tausk, Phys. Lett. B469 (1999) 225–234, [hep-ph/9909506](#).
77. V. Smirnov and O. Veretin, Nucl. Phys. B566 (2000) 469–485, [hep-ph/9907385](#).
78. V. A. Smirnov, Phys. Lett. B524 (2002) 129–136, [hep-ph/0111160](#).
79. G. Heinrich and V. A. Smirnov, Phys. Lett. B598 (2004) 55–66, [hep-ph/0406053](#).
80. M. Czakon, Comput. Phys. Commun. 175 (2006) 559–571, [hep-ph/0511200](#).
81. J. Gluza, K. Kajda, and T. Riemann, Comput. Phys. Commun. 177 (2007) 879–893, [arXiv:0704.2423](#).
82. A. Goncharov, Math. Res. Letters 5 (1998) 497.
83. D. J. Broadhurst, Eur. Phys. J. C8 (1999) 311–333, [hep-th/9803091](#).
84. E. Remiddi and J. Vermaseren, Int. J. Mod. Phys. A15 (2000) 725–754, [hep-ph/9905237](#).
85. T. Gehrmann and E. Remiddi, Comput. Phys. Commun. 141 (2001) 296–312, <http://arXiv.org/abs/hep-ph/0107173>.
86. T. Gehrmann and E. Remiddi, Comput. Phys. Commun. 144 (2002) 200–223, [hep-ph/0111255](#).
87. D. Maitre, Comput. Phys. Commun. 174 (2006) 222–240, [hep-ph/0507152](#).
88. D. Maitre, [hep-ph/0703052](#).
89. J. Vollinga and S. Weinzierl, Comput. Phys. Commun. 167 (2005) 177, [hep-ph/0410259](#).
90. S. Weinzierl, [0705.0900](#).
91. A. A. Penin, Phys. Rev. Lett. 95 (2005) 010408, [hep-ph/0501120](#).
92. A. A. Penin, Nucl. Phys. B734 (2006) 185–202, [hep-ph/0508127](#).
93. A. Mitov and S. Moch, JHEP 05 (2007) 001, [hep-ph/0612149](#).
94. T. Becher and K. Melnikov, JHEP 06 (2007) 084, [arXiv:0704.3582 \[hep-ph\]](#).
95. Z. Bern, L. Dixon, and A. Ghinculov, Phys. Rev. D63 (2001) 053007, [hep-ph/0010075](#).
96. R. Bonciani and A. Ferroglia, Phys. Rev. D72 (2005) 056004, [hep-ph/0507047](#).
97. R. Bonciani, P. Mastrolia, and E. Remiddi, Nucl. Phys. B661 (2003) 289–343, [hep-ph/0301170](#).
98. M. Czakon, J. Gluza, and T. Riemann, Phys. Rev. D71 (2005) 073009, [hep-ph/0412164](#).
99. M. Czakon, J. Gluza, and T. Riemann, Nucl. Phys. B751 (2006) 1–17, [hep-ph/0604101](#).
100. D. J. Broadhurst, J. Fleischer, and O. V. Tarasov, Z. Phys. C60 (1993) 287–302, [hep-ph/9304303](#).
101. A. I. Davydychev and M. Y. Kalmykov, Nucl. Phys. B699 (2004) 3–64, [hep-th/0303162](#).
102. A. B. Arbuzov, E. A. Kuraev, and B. G. Shaikhadenov, Mod. Phys. Lett. A13 (1998) 2305–2316, [hep-ph/9806215](#).
103. E. W. N. Glover, J. B. Tausk, and J. J. Van der Bij, Phys. Lett. B516 (2001) 33–38, [hep-ph/0106052](#).
104. G. J. H. Burgers, Phys. Lett. B164 (1985) 167.
105. R. Bonciani, A. Ferroglia, P. Mastrolia, E. Remiddi, and J. van der Bij, Nucl. Phys. B681 (2004) 261–291, [hep-ph/0310333](#).
106. R. Bonciani, A. Ferroglia, P. Mastrolia, E. Remiddi, and J. van der Bij, Nucl. Phys. B701 (2004) 121–179, [hep-ph/0405275](#).
107. R. Bonciani, A. Ferroglia, P. Mastrolia, E. Remiddi, and J. van der Bij, [hep-ph/0411321](#).
108. S. Actis, M. Czakon, J. Gluza, and T. Riemann, Nucl. Phys. B786 (2007) 26–51, [arXiv:0704.2400v.2 \[hep-ph\]](#).
109. A. B. Arbuzov, E. A. Kuraev, N. P. Merenkov, and L. Trentadue, Phys. Atom. Nucl. 60 (1997) 591–600.
110. R. Bonciani, A. Ferroglia, and A. A. Penin, Phys. Rev. Lett. 100 (2008) 131601, [0710.4775](#).
111. R. Bonciani, A. Ferroglia, and A. A. Penin, JHEP 02 (2008) 080, [arXiv:0802.2215](#).
112. S. Actis, M. Czakon, J. Gluza, and T. Riemann, Phys. Rev. Lett. 100 (2008) 131602, [arXiv:0711.3847](#).
113. S. Actis, M. Czakon, J. Gluza, and T. Riemann, Phys. Rev. D78 (2008) 085019, [arXiv:0807.4691](#).
114. J. Frenkel and J. C. Taylor, Nucl. Phys. B116 (1976) 185.
115. J. Fleischer, A. V. Kotikov, and O. L. Veretin, Nucl. Phys. B547 (1999) 343–374, [hep-ph/9808242](#).
116. U. Aglietti and R. Bonciani, Nucl. Phys. B668 (2003) 3–76, [hep-ph/0304028](#).
117. U. Aglietti and R. Bonciani, Nucl. Phys. B698 (2004) 277–318, [hep-ph/0401193](#).
118. R. E. Cutkosky, J. Math. Phys. 1 (1960) 429–433.
119. M. Davier, S. Eidelman, A. Höcker, and Z. Zhang, Eur. Phys. J. C27 (2003) 497–521, [hep-ph/0208177](#).
120. Private communications with T. Teubner. The Fortran program rintpl.F is based on the data compilation performed for [219, 220]. The publication is in preparation. The routine is available upon request from the authors, E-mails: dnomura@post.kek.jp, thomas.teubner@liverpool.ac.uk.
121. R. V. Harlander and M. Steinhauser, Comput. Phys. Commun. 153 (2003) 244–274, [hep-ph/0212294](#).
122. F. Berends and G. Komen, Phys. Lett. B63 (1976) 432.
123. B. Kniehl, M. Krawczyk, J. Kühn, and R. Stuart, Phys. Lett. B209 (1988) 337.
124. T. van Ritbergen and R. G. Stuart, Phys. Lett. B437 (1998) 201–208, [hep-ph/9802341](#).
125. S. Actis, M. Czakon, J. Gluza, and T. Riemann, Acta Phys. Polon. B38 (2007) 3517–3528, [arXiv:0710.5111](#).

126. J. H. Kühn and S. Uccirati, Nucl. Phys. B806 (2009) 300–326, [arXiv:0807.1284](#).
127. DESY Zeuthen webpage [bhabha.html](#).
128. H. Burkhardt, [TASSO-NOTE-192 \(1981\)](#), and Fortran program [repi.f](#) (1986).
129. G. Passarino and M. Veltman, Nucl. Phys. B160 (1979) 151.
130. Z. Bern, L. J. Dixon, and D. A. Kosower, Ann. Rev. Nucl. Part. Sci. 46 (1996) 109–148, [hep-ph/9602280](#).
131. L. J. Dixon, [hep-ph/9601359](#).
132. T. Binoth, J. P. Guillet, and G. Heinrich, Nucl. Phys. B572 (2000) 361–386, [hep-ph/9911342](#).
133. A. Denner and S. Dittmaier, Nucl. Phys. B658 (2003) 175–202, [hep-ph/0212259](#).
134. T. Binoth, J. P. Guillet, G. Heinrich, E. Pilon, and C. Schubert, JHEP 10 (2005) 015, [hep-ph/0504267](#).
135. A. Denner and S. Dittmaier, Nucl. Phys. B734 (2006) 62–115, [hep-ph/0509141](#).
136. A. Denner and S. Dittmaier, Nucl. Phys. Proc. Suppl. 157 (2006) 53–57, [hep-ph/0601085](#).
137. A. Davydychev, Phys. Lett. B263 (1991) 107–111.
138. O. V. Tarasov, Phys. Rev. D54 (1996) 6479–6490, [http://arXiv.org/abs/hep-th/9606018](#).
139. J. Fleischer, F. Jegerlehner, and O. Tarasov, Nucl. Phys. B566 (2000) 423–440, [http://arXiv.org/abs/hep-ph/9907327](#).
140. D. B. Melrose, Nuovo Cim. 40 (1965) 181–213.
141. T. Diakonidis, J. Fleischer, J. Gluza, K. Kajda, T. Riemann, and J. Tausk, [arXiv:0807.2984](#).
142. T. Diakonidis, J. Fleischer, J. Gluza, K. Kajda, T. Riemann, and J. Tausk, [0812.2134](#).
143. Z. Bern, L. J. Dixon, and D. A. Kosower, Annals Phys. 322 (2007) 1587–1634, [0704.2798](#).
144. L. D. Landau, Nucl. Phys. 13 (1959) 181–192.
145. S. Mandelstam, Phys. Rev. 112 (1958) 1344–1360.
146. S. Mandelstam, Phys. Rev. 115 (1959) 1741–1751.
147. R. J. Eden, P. V. Landshoff, D. I. Olive, and J. C. Polkinghorne, Cambridge University Press (1966).
148. G. 't Hooft and M. Veltman, Nucl. Phys. B153 (1979) 365–401.
149. Z. Bern, L. J. Dixon, and D. A. Kosower, Phys. Lett. B302 (1993) 299–308, [hep-ph/9212308](#).
150. Z. Bern, L. J. Dixon, and D. A. Kosower, Nucl. Phys. B412 (1994) 751–816, [hep-ph/9306240](#).
151. G. Duplancic and B. Nizic, Eur. Phys. J. C35 (2004) 105–118, [hep-ph/0303184](#).
152. R. K. Ellis and G. Zanderighi, JHEP 02 (2008) 002, [0712.1851](#).
153. R. Britto, F. Cachazo, and B. Feng, Nucl. Phys. B725 (2005) 275–305, [hep-th/0412103](#).
154. P. Mastrolia, Phys. Lett. B644 (2007) 272–283, [hep-th/0611091](#).
155. D. Forde, Phys. Rev. D75 (2007) 125019, [0704.1835](#).
156. N. E. J. Bjerrum-Bohr, D. C. Dunbar, and W. B. Perkins, JHEP 04 (2008) 038, [0709.2086](#).
157. R. Britto, E. Buchbinder, F. Cachazo, and B. Feng, Phys. Rev. D72 (2005) 065012, [hep-ph/0503132](#).
158. R. Britto, B. Feng, and P. Mastrolia, Phys. Rev. D73 (2006) 105004, [hep-ph/0602178](#).
159. C. Anastasiou, R. Britto, B. Feng, Z. Kunszt, and P. Mastrolia, Phys. Lett. B645 (2007) 213–216, [hep-ph/0609191](#).
160. C. Anastasiou, R. Britto, B. Feng, Z. Kunszt, and P. Mastrolia, JHEP 03 (2007) 111, [hep-ph/0612277](#).
161. R. Britto and B. Feng, Phys. Rev. D75 (2007) 105006, [hep-ph/0612089](#).
162. E. W. Nigel Glover and C. Williams, JHEP 12 (2008) 067, [0810.2964](#).
163. R. Britto, B. Feng, and P. Mastrolia, Phys. Rev. D78 (2008) 025031, [0803.1989](#).
164. G. Ossola, C. G. Papadopoulos, and R. Pittau, Nucl. Phys. B763 (2007) 147–169, [hep-ph/0609007](#).
165. G. Ossola, C. G. Papadopoulos, and R. Pittau, JHEP 07 (2007) 085, [0704.1271](#).
166. F. del Aguila and R. Pittau, JHEP 07 (2004) 017, [hep-ph/0404120](#).
167. R. Pittau, [hep-ph/0406105](#).
168. R. Pittau, Comput. Phys. Commun. 104 (1997) 23–36, [hep-ph/9607309](#).
169. R. Pittau, Comput. Phys. Commun. 111 (1998) 48–52, [hep-ph/9712418](#).
170. P. Mastrolia, G. Ossola, C. G. Papadopoulos, and R. Pittau, JHEP 06 (2008) 030, [0803.3964](#).
171. G. Ossola, C. G. Papadopoulos, and R. Pittau, JHEP 05 (2008) 004, [0802.1876](#).
172. A. Kanaki and C. G. Papadopoulos, Comput. Phys. Commun. 132 (2000) 306–315, [hep-ph/0002082](#).
173. C. G. Papadopoulos, Comput. Phys. Commun. 137 (2001) 247–254, [hep-ph/0007335](#).
174. C. G. Papadopoulos and M. Worek, Eur. Phys. J. C50 (2007) 843–856, [hep-ph/0512150](#).
175. A. Cafarella, C. G. Papadopoulos, and M. Worek, [0710.2427](#).
176. H. Czyz, A. Grzelinska, and A. Wapienik, Acta Phys. Polon. B38 (2007) 3491, [0710.4227](#).
177. H. Czyz, Nucl. Phys. Proc. Suppl. 181–182 (2008) 264–268.
178. G. Montagna, M. Moretti, O. Nicrosini, A. Pallavicini, and F. Piccinini, Nucl. Phys. B547 (1999) 39–59, [hep-ph/9811436](#).
179. E. Kuraev and V. Fadin, Sov. J. Nucl. Phys. 41 (1985) 466.
180. G. Altarelli and G. Martinelli, In *Ellis, J. (Ed.), Peccei, R.d. (Ed.): Physics At Lep, Vol. 1*, 47–57.
181. O. Nicrosini and L. Trentadue, Phys. Lett. B196 (1987) 551.
182. O. Nicrosini and L. Trentadue, Z. Phys. C39 (1988) 479.
183. D. Yennie, S. Frautschi, and H. Suura, Annals Phys. 13 (1961) 379.
184. C. M. Carloni Calame, C. Lunardini, G. Montagna, O. Nicrosini, and F. Piccinini, Nucl. Phys. B584 (2000) 459–479, [hep-ph/0003268](#).
185. C. M. Carloni Calame, G. Montagna, O. Nicrosini, and F. Piccinini, Nucl. Phys. Proc. Suppl. 131 (2004) 48–55, [hep-ph/0312014](#).
186. G. Balossini, C. M. Carloni Calame, G. Montagna, O. Nicrosini, and F. Piccinini, Nucl. Phys. B758 (2006) 227–253, [hep-ph/0607181](#).
187. A. B. Arbuzov, G. V. Fedotov, F. V. Ignatov, E. A. Kuraev, and A. L. Sibidanov, Eur. Phys. J. C46 (2006) 689–703, [hep-ph/0504233](#).
188. S. Jadach, W. Placzek, and B. F. L. Ward, Phys. Lett. B390 (1997) 298–308, [hep-ph/9608412](#).
189. V. Gribov and L. Lipatov, Sov. J. Nucl. Phys. 15 (1972) 675.

190. G. Altarelli and G. Parisi, Nucl. Phys. B126 (1977) 298.
191. Y. Dokshitzer, Sov. Phys. JETP 46 (1977) 641.
192. M. Cacciari, A. Deandrea, G. Montagna, and O. Nicrosini, Europhys. Lett. 17 (1992) 123.
193. M. Skrzypek, Acta Phys. Polon. B24 (1992) 123.
194. M. Przybycien, Acta Phys. Polon. B24 (1993) 1105.
195. A. B. Arbuzov, Phys. Lett. B470 (1999) 252.
196. A. Arbuzov, G. Fedotov, E. Kuraev, N. Merenkov, V. Rushai, and L. Trentadue, JHEP 9710 (1997) 001, [9702262](#).
197. A. B. Arbuzov and E. Scherbakova, JETP Lett. 83 (2006) 427.
198. M. Greco and O. Nicrosini, Phys. Lett. B240 (1990) 219.
199. C. M. Carloni Calame, Phys. Lett. B520 (2001) 16–24, [hep-ph/0103117](#).
200. G. Montagna, O. Nicrosini, and F. Piccinini, Phys. Lett. B385 (1996) 348–356, [hep-ph/9605252](#).
201. S. Frixione and B. R. Webber, JHEP 06 (2002) 029, [hep-ph/0204244](#).
202. P. Nason, JHEP 11 (2004) 040, [hep-ph/0409146](#).
203. S. Frixione, P. Nason, and C. Oleari, JHEP 11 (2007) 070, [0709.2092](#).
204. S. Alioli, P. Nason, C. Oleari, and E. Re, JHEP 07 (2008) 060, [0805.4802](#).
205. C. M. Carloni Calame, G. Montagna, O. Nicrosini, and A. Vicini, JHEP 12 (2006) 016, [hep-ph/0609170](#).
206. C. M. Carloni Calame, G. Montagna, O. Nicrosini, and A. Vicini, JHEP 10 (2007) 109, [0710.1722](#).
207. A. B. Arbuzov and E. Scherbakova, Phys. Lett. B660 (2008) 37.
208. E. Drago and G. Venanzoni, [KLOE note INFN/AE-97/48](#).
209. F. Berends and R. Kleiss, Nucl. Phys. B228 (1983) 537.
210. F. Berends and R. Kleiss, Nucl. Phys. B186 (1981) 22.
211. F. Jegerlehner, Z. Phys. C32 (1986) 195.
212. H. Burkhardt, F. Jegerlehner, G. Penso, and C. Verzegnassi, Z. Phys. C43 (1989) 497–501.
213. G. Balossini et al., Phys. Lett. B663 (2008) 209–213, [0801.3360](#).
214. P. Rong-Gang, [Private communication](#).
215. S. Jadach, M. Melles, B. F. L. Ward, and S. A. Yost, Phys. Lett. B377 (1996) 168–176, [hep-ph/9603248](#).
216. B. F. L. Ward, S. Jadach, M. Melles, and S. A. Yost, Phys. Lett. B450 (1999) 262–266, [hep-ph/9811245](#).
217. C. Glosser, S. Jadach, B. F. L. Ward, and S. A. Yost, Phys. Lett. B605 (2005) 123–128, [hep-ph/0406298](#).
218. S. Jadach, B. F. L. Ward, and S. A. Yost, Phys. Rev. D73 (2006) 073001, [hep-ph/0602197](#).
219. K. Hagiwara, A. D. Martin, D. Nomura, and T. Teubner, Phys. Rev. D69 (2004) 093003, [hep-ph/0312250](#).
220. K. Hagiwara, A. D. Martin, D. Nomura, and T. Teubner, Phys. Lett. B649 (2007) 173–179, [hep-ph/0611102](#).